Eur. Phys. J. C (2020) 80:467
https://doi.org/10.1140/epjc/s10052-020-8028-1

THE EUROPEAN PHYSICAL JOURNAL C

Regular Article - Theoretical Physics

tZ' production at hadron colliders

Marco Guzzi[a], **Nikolaos Kidonakis**[b]

Department of Physics, Kennesaw State University, Kennesaw, GA 30144, USA

Received: 23 January 2020 / Accepted: 8 May 2020 / Published online: 25 May 2020

Abstract We study the production of a single top quark in association with a heavy extra Z' at hadron colliders in new physics models with and without flavor-changing neutral-current (FCNC) couplings. We use QCD soft-gluon resummation and threshold expansions to calculate higher-order corrections for the total cross section and transverse-momentum distributions for tZ' production. The impact of the uncertainties due to the structure of the proton and scale dependence is also analyzed.

1 Introduction

The top quark is the heaviest particle in the three quark generations. Its mass of approximately $m_t = 172.5$ GeV has been measured with very high accuracy at the Large Hadron Collider (LHC) [1–3], and being close to that of the Higgs boson it makes the top quark one of the best candidates to probe the Electroweak (EW) sector of the Standard Model (SM) and its extensions.

The accumulated data at the LHC have not yet provided us with evidence of deviations from the SM, but Run II of the LHC and its upgrade to a High Luminosity phase (HL-LHC) [4], and especially future center-of-mass energy upgrades are going to record a large number of high-energy collision data which will allow us to probe rare processes that may hint at or provide direct evidence of new physics. In particular, for physics Beyond the Standard Model (BSM) and beyond the LHC, there are several projects going on which provide a synergy of various new-generation facilities like the Future Circular Collider (FCC) [5–7] and the Super proton proton Collider (SppC) [8]. With a center-of-mass energy of approximately 100 TeV, these new-generation hadron colliders represent the new frontier for discovery at high energies and will be critical to identify particles with mass of $\mathcal{O}(10)$ TeV. At these energies, we will be able to investigate properties of the Higgs boson and the top quark, and EW symmetry-breaking phenomena with unprecedented precision and sensitivity. Moreover, the statistics will be enhanced by several orders of magnitude with respect to that of the LHC, and this is going to be ideal to study BSM physics and rare processes. In this respect, a process of interest is the production of a single top quark in association with a new heavy particle.

Regardless of the type of the new heavy particle, many aspects of this reaction are interesting at quantum-field-theoretical level and because of the phenomenological implications on BSM physics. For example, the kinematics of the final state and decay products can be relevant to investigate extensions of the Higgs sector (two-Higgs-doublet model (2HDM), SUSY, etc.), and of the EW sector with enlarged gauge symmetry.

In this work we shall focus on the production of a top quark in association with an extra Z' vector boson coming from distinct BSM theories, and we will analyze higher-order QCD corrections to this process due to soft gluon emissions.

Extra vector gauge bosons, generically referred to as extra Z's, are almost ubiquitous in extensions of the EW sector of the SM. Z's are associated with additional abelian $U'(1)$ gauge symmetries which were suggested in SM extensions such as left-right symmetric models, Grand Unified Theories (GUTs) and string-inspired constructions (see Refs. [9–14] for reviews and references). In the past decade, Z' gauge bosons at the TeV scale gathered considerable attention in theoretical calculations (including parton-shower) [15–20] and triggered a vigorous program of experimental searches at the LHC. At high energies, Z's can in principle have different signatures: they can be produced as intermediate resonances in Drell–Yan processes as well as in association with another SM vector or scalar boson, or in association with a jet or single top quark such as in the case of $pp \to tZ'$.

The dynamics of this process is non-trivial because of several hard scales entering the cross section. In fact, in

[a] e-mail: mguzzi@kennesaw.edu (corresponding author)
[b] e-mail: nkidonak@kennesaw.edu

high-energy reactions in which the final-state heavy particle has a mass much heavier than the top quark mass, m_t, the cross section is affected by large (collinear) logarithmic contributions of the type $\alpha_s^n \log^n \left(Q^2/m_t^2\right)$ (where $Q \approx m_{Z'}$, the Z'-boson mass, and α_s is the QCD coupling constant) that can spoil the convergence of the perturbative series in calculations at fixed order [21]. Therefore, there is the necessity of resumming these logarithmic contributions using DGLAP evolution defining a top-quark parton distribution function (PDF) inside the proton. When a higher energy scale $Q \approx m_{Z'}$ involving a heavy final state is such that $m_{Z'} \gg m_t$, the top quark can be considered essentially massless and an active flavor inside the proton. Details of factorization schemes with different number of flavors with consistent treatment of the top quark as a massless degree of freedom at high energies are discussed in Refs. [22,23] and references therein. In particular, QCD factorization with initial-state heavy flavors is discussed in Refs. [24–28].

In processes with very heavy final states the near-threshold kinematic region becomes particularly important. Soft-gluon corrections typically become large and dominant in such circumstances. Therefore, the K-factors can become quite large and it is important to include these corrections in making theoretical predictions. In this study, we adopt and extend the soft-gluon resummation formalism used in [29–31] for tZ and $t\gamma$ production (see also applications to top–antitop pair production [32–34] and single-top production [35–39], and a review in [40]) to calculate approximate next-to-next-to-leading order (aNNLO) cross sections for tZ' associated production in two case scenarios: (i) the case of Z's with flavor-changing anomalous couplings, (ii) the case of Z's originating from low-energy realizations of string models. We explore the impact of the corrections due to multiple emission of soft-gluons as well as the cross section suppression due to Z's of different mass and couplings. Moreover, we analyze the uncertainties in the cross section associated to the PDFs of the initial state protons and to the factorization μ_F and renormalization μ_R scales. Finally, we generate prospects for the cross section for the case studies mentioned above, at future generation ultra-high energy colliders.

The paper is organized as follows. In Sect. 2 we discuss the BSM effective Lagrangians, couplings, and leading-order cross sections. In Sect. 3 we illustrate the soft-gluon formalism and calculate the higher-order corrections. In Sect. 4 we present results for the total cross sections and top-quark transverse-momentum (p_T) distributions in tZ' production via the processes $gu \to tZ'$ and $gc \to tZ'$ with anomalous couplings, and also via the process $gt \to tZ'$. We conclude in Sect. 5.

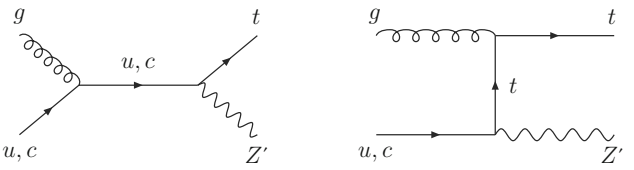

Fig. 1 Leading-order diagrams for $gu \to tZ'$ with anomalous t–u–Z' coupling and $gc \to tZ'$ with anomalous t–c–Z' coupling

2 Effective Lagrangians

2.1 Lagrangian for FCNC Z's

An FCNC term in the Lagrangian that includes the anomalous coupling of a t, q pair to a Z' boson is given by

$$\mathcal{L}_{FCNC} = \frac{1}{\Lambda} \kappa_{tqZ'}\, e\, \bar{t}\, \sigma_{\mu\nu}\, q\, F_{Z'}^{\mu\nu} + h.c., \tag{2.1}$$

where $\kappa_{tqZ'}$ is the anomalous t–q–Z' coupling, with q an up or charm quark; e is the electron charge; Λ is an effective new physics scale in the few TeV's range; $F_{Z'}^{\mu\nu}$ is the Z' field tensor; and $\sigma_{\mu\nu} = (i/2)(\gamma_\mu\gamma_\nu - \gamma_\nu\gamma_\mu)$ with γ_μ the Dirac matrices.

The partonic processes involved are $gu \to tZ'$ and $gc \to tZ'$. Leading-order diagrams for these processes are shown in Fig. 1. Related processes involving Z bosons with anomalous couplings were studied in Refs. [29,30].

2.2 Lagrangian for string-inspired Z's

The Lagrangian for a Z' coming from string-inspired models is given below, where we adopt the notation introduced in Refs. [41,42]. Here we report the most basic definitions for completeness.

The fermion-fermion-Z' interaction is given by

$$\sum_{i=L,R} z_{t,i}\, g_{Z'} \bar{t}_i \gamma^\mu t_i\, Z'_\mu, \tag{2.2}$$

where the coefficients $z_{t,L}$, and $z_{t,R}$ are the charges of the left- and right-handed top quarks respectively. The Z' coupling is indicated by $g_{Z'}$.

The mass of the Z gauge boson is parametrized in terms of the vacuum expectation values (vev's) of the Higgs sector v_{H_1}, v_{H_2} as follows

$$\begin{aligned} m_Z^2 &= \frac{g^2}{4\cos^2\theta_W}(v_{H_1}^2 + v_{H_2}^2)\left[1 + O(\varepsilon^2)\right], \\ \varepsilon &= \frac{\delta m_{ZZ'}^2}{m_{Z'}^2 - m_Z^2}, \\ \delta m_{ZZ'}^2 &= -\frac{g g_{Z'}}{4\cos\theta_W}(z_{H_1}^2 v_{H_1}^2 + z_{H_2}^2 v_{H_2}^2), \end{aligned} \tag{2.3}$$

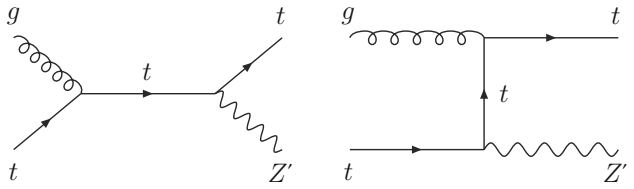

Fig. 2 Leading-order diagrams for $gt \to tZ'$

where the mixing parameter ε is defined perturbatively, z_{H_1} and z_{H_2} are the charges of the Higgses, $g = e/\sin\theta_W$, $g_Y = e/\cos\theta_W$, and θ_W is the Weinberg angle. We consider $m_{Z'}$ as a free parameter in the TeV's range. We restrict our attention to the interaction Lagrangian for the top-quark sector only, which is written as

$$\mathcal{L}_{int} = \bar{t}_L N_L^{Z'} \gamma^\mu t_L Z'_\mu + \bar{t}_R N_R^{Z'} \gamma^\mu t_R Z'_\mu, \tag{2.4}$$

where the left-handed (L) and right-handed (R) couplings are

$$\begin{aligned} N_L^{Z'} &= -i\left(-g\cos\theta_W T_{3,L}\varepsilon + g_Y \sin\theta_W \frac{Y_{t,L}}{2}\varepsilon + g_{Z'}\frac{z_{t,L}}{2}\right), \\ N_R^{Z'} &= -i\left(g_Y \sin\theta_W \frac{Y_{t,R}}{2}\varepsilon + g_{Z'}\frac{z_{t,R}}{2}\right), \end{aligned} \tag{2.5}$$

where $Y_{t,L/R}$ is the hypercharge and $T_{3,L}$ is the weak isospin.

Based on this Lagrangian, we will study below the process $gt \to tZ'$. The leading-order diagrams for this process are shown in Fig. 2.

2.3 Hadronic cross section

The hadronic cross section for $p(P_1) + p(P_2) \to t(p_t) + Z'(p_{Z'})$ is expressed in terms of Mandelstam variables

$$\begin{aligned} &S = (P_1 + P_2)^2, \quad T = (P_1 - p_t)^2, \quad U = (P_2 - p_t)^2, \\ &S_4 = S + T + U - m_t^2 - m_{Z'}^2. \end{aligned} \tag{2.6}$$

We also define $T_1 = T - m_t^2$ and $U_1 = U - m_t^2$.

The factorized differential cross section can be written as

$$\begin{aligned} &S^2 \frac{d^2\sigma(S, T_1, U_1)}{dT_1\, dU_1} \\ &= \sum_{i,j=q,g} \int_{x_1^-}^1 \frac{dx_1}{x_1} \int_{x_2^-}^1 \frac{dx_2}{x_2} f_{i/p_1}(x_1, \mu_F^2) f_{j/p_2}(x_2, \mu_F^2) \\ &\quad \times \hat{\sigma}_{ij\to tZ'}(s, t_1, u_1, m_t^2, m_{Z'}^2, \mu_F^2, \alpha_s(\mu_R^2)) \\ &\quad + \mathcal{O}(\Lambda_{QCD}^2/\Lambda^2) \end{aligned} \tag{2.7}$$

where $f_{j/p}(x, \mu_F^2)$ is the parton distribution function representing the probability of finding the parton j in proton p, μ_F and μ_R are the factorization and renormalization scales respectively, and $\hat{\sigma}_{ij\to tZ'}$ is the hard scattering cross section. Here, Λ_{QCD} is the QCD scale while the scale Λ is of the order of $m_{Z'}$, and power suppressed terms $\Lambda_{QCD}^2/\Lambda^2$ are neglected. In our numerical results in Sect. 4 we set $\mu_F = \mu_R = \mu$.

The lower integration limits in the factorization formula are given by

$$x_1^- = -\frac{U_1}{S + T_1}, \quad x_2^- = -\frac{x_1 T_1}{x_1 S + U_1}. \tag{2.8}$$

The double-differential cross section in Eq. (2.7) can be written in terms of the transverse momentum p_T of the top quark and its rapidity y using

$$T_1 = -\sqrt{S}\, m_T e^{-y}, \quad U_1 = -\sqrt{S}\, m_T e^{y}, \tag{2.9}$$

where the transverse mass m_T is defined as $m_T = \sqrt{p_T^2 + m_t^2}$.

2.4 Leading-order cross sections

For the partonic process $g(p_g) + q(p_q) \to t(p_t) + Z'(p_{Z'})$, we define the kinematical variables $s = (p_g + p_q)^2$, $t = (p_g - p_t)^2$, and $u = (p_q - p_t)^2$.

The leading-order (LO) double-differential partonic cross section for $gq \to tZ'$, with q and up or charm quark, via anomalous couplings is

$$\frac{d^2\hat{\sigma}^{(0)}_{gq\to tZ'}}{dt\, du} = F^{\rm LO}_{gq\to tZ'}\, \delta(s_4), \tag{2.10}$$

where

$$\begin{aligned} &F^{\rm LO}_{gq\to tZ'} \\ &= \frac{2\pi\alpha\alpha_s \kappa_{tqZ'}^2}{3s^3(t - m_t^2)^2\Lambda^2}\Big\{2m_t^8 - m_t^6(3m_{Z'}^2 + 4s + 2t) \\ &\quad + m_t^4\left[2m_{Z'}^4 - m_{Z'}^2(2s + t) + 2(s^2 + 4st + t^2)\right] \\ &\quad + m_t^2\left[2m_{Z'}^6 - 4m_{Z'}^4 t + m_{Z'}^2(s + t)(s + 5t)\right. \\ &\quad \left. - 2t(3s^2 + 6st + t^2)\right] - t\left[2m_{Z'}^6 - 2m_{Z'}^4(s + t)\right. \\ &\quad \left. + m_{Z'}^2(s + t)^2 - 4st(s + t)\right]\Big\}, \end{aligned} \tag{2.11}$$

with $\alpha = e^2/(4\pi)$.

For the partonic process $g(p_g) + t(p_q) \to t(p_t) + Z'(p_{Z'})$, we again define the kinematical variables $s = (p_g + p_q)^2$, $t = (p_g - p_t)^2$, and $u = (p_q - p_t)^2$. The LO cross section for $gt \to tZ'$ is given by

$$\begin{aligned} &F^{\rm LO}_{gt\to tZ'} \\ &= 4\frac{4\pi\alpha_s}{m_{Z'}^2 N_c (s - m_t^2)^2 (t - m_t^2)^2}\Big\{g_{AtZ'}^2\Big[2m_{Z'}^4((2m_t^2 st \\ &\quad - 5m_t^4(s + t) + 6m_t^6) + st(s + t)) \\ &\quad + 2m_{Z'}^6(s - m_t^2)(m_t^2 - t) - m_{Z'}^2(m_t^4(s - 3t)(3s - t) \\ &\quad - 12m_t^6(s + t) - m_t^2(s + t)(-6st + s^2 + t^2) \end{aligned}$$

$$
\begin{aligned}
&+18m_t^8 + st(s^2+t^2)) \\
&-2m_t^2(s-m_t^2)(t-m_t^2)(-2m_t^2+s+t)^2\Big] \\
&+g_{VtZ'}^2 m_{Z'}^2\Big[-st(2m_{Z'}^4+s^2+t^2 \\
&-2m_{Z'}^2(s+t)) - m_t^4(-2m_{Z'}^2(s+t) \\
&+2m_{Z'}^4+14st+3s^2+3t^2) \\
&+m_t^2(-8m_{Z'}^2 st + 2m_{Z'}^4(s+t) + (s+t) \\
&\quad (6st+s^2+t^2)) + 6m_t^8\Big]\Big\}, \qquad (2.12)
\end{aligned}
$$

where the vector and axial coupling of the Z' boson to the top quark are

$$
\begin{aligned}
\frac{-ig}{4c_w}\gamma^\mu g_{VtZ'} &= \frac{-ig}{c_w}\frac{1}{2}\Big[-\varepsilon c_w^2 T_3^L + \varepsilon s_w^2\Big(\frac{Y_{t,L}}{2} \\
&\quad + \frac{Y_{t,R}}{2}\Big) + \frac{g_{Z'}}{g} c_w\Big(\frac{z_{t,L}}{2}+\frac{z_{t,R}}{2}\Big)\Big]\gamma^\mu \\
\frac{-ig}{4c_w}\gamma^\mu\gamma^5 g_{AtZ'} &= \frac{-ig}{c_w}\frac{1}{2}\Big[\varepsilon c_w^2 T_3^L + \varepsilon s_w^2\Big(\frac{Y_{t,R}}{2}-\frac{Y_{t,L}}{2}\Big) \\
&\quad + \frac{g_{Z'}}{g} c_w\Big(\frac{z_{t,R}}{2}-\frac{z_{t,L}}{2}\Big)\Big]\gamma^\mu\gamma^5, \qquad (2.13)
\end{aligned}
$$

where we set $\sin\theta_W = s_w$ and $\cos\theta_W = c_w$ for brevity.

3 Soft-gluon corrections

We next describe the formalism and procedure for calculating soft-gluon corrections in the cross section for tZ' production. For the processes $gq \to tZ'$ and $gt \to tZ'$, we defined the usual kinematical variables s, t, and u, in the previous section. We can also define a threshold kinematical variable, $s_4 = s+t+u-m_t^2-m_{Z'}^2$, that measures distance from partonic threshold, and vanishes at partonic threshold where there is no energy available for additional radiation. More specifically, s_4 is the squared invariant mass of additional final-state radiation. We also define $t_1 = t - m_t^2$, $t_2 = t - m_{Z'}^2$, $u_1 = u - m_t^2$, and $u_2 = u - m_{Z'}^2$.

The resummation of soft-gluon contributions to the partonic process follows from the factorization of the cross section as a product of functions that describe soft and collinear emission. Taking the Laplace transform $\hat{\sigma}(N) = \int (ds_4/s)\, e^{-Ns_4/s}\hat{\sigma}(s_4)$, we have a factorized expression in $4-\epsilon$ dimensions,

$$
\begin{aligned}
\frac{d^2\hat{\sigma}_{gq\to tZ'}(N,\epsilon)}{dt\,du} &= H_{gq\to tZ'}(\alpha_s(\mu)) \times \\
S_{gq\to tZ'}&\left(\frac{m_t}{N\mu},\alpha_s(\mu)\right)\prod_{i=g,q} J_i(N,\mu,\epsilon) \qquad (3.1)
\end{aligned}
$$

where $H_{gq\to tZ'}$ is a hard function, $S_{gq\to tZ'}$ is a soft function for noncollinear soft-gluon emission, and J_i are jet functions for soft and collinear emission from the incoming quark and gluon. Our considerations are identical for all three processes to be studied in this paper, i.e. $gu \to tZ'$, $gc \to tZ'$, and $gt \to tZ'$.

The dependence of the soft function $S_{gq\to tZ}$ on N is resummed via renormalization group evolution [30–39,43],

$$
S^b_{gq\to tZ'} = (Z^S)^*\, S_{gq\to tZ'}\, Z^S, \qquad (3.2)
$$

with $S^b_{gq\to tZ}$ the unrenormalized quantity and Z^S a renormalization constant. The function $S_{gq\to tZ}$ obeys the renormalization group equation

$$
\left(\mu\frac{\partial}{\partial\mu} + \beta(g_s,\epsilon)\frac{\partial}{\partial g_s}\right) S_{gq\to tZ'} = -2\, S_{gq\to tZ'}\,\Gamma^S_{gq\to tZ'}, \qquad (3.3)
$$

where $g_s^2 = 4\pi\alpha_s$, $\beta(g_s,\epsilon) = -g_s\epsilon/2 + \beta(g_s)$ with $\beta(g_s)$ the QCD beta function, and

$$
\Gamma^S_{gq\to tZ'} = \frac{dZ^S}{d\ln\mu}(Z^S)^{-1} = \beta(g_s,\epsilon)\frac{\partial Z^S}{\partial g_s}(Z^S)^{-1} \qquad (3.4)
$$

is the soft anomalous dimension that determines the evolution of $S_{gq\to tZ}$. The soft anomalous dimension $\Gamma^S_{gq\to tZ}$ is calculated in dimensional regularization from the coefficients of the ultraviolet poles of the loop diagrams involved in the process [30–40,43–45].

The resummed partonic cross section in moment space is then given by

$$
\begin{aligned}
&\frac{d^2\hat{\sigma}^{\text{resum}}_{gq\to tZ}(N)}{dt\,du} \\
&= \exp\left[\sum_{i=g,q} E_i(N_i)\right] H_{gq\to tZ'}\left(\alpha_s(\sqrt{s})\right) \\
&\quad \times S_{gq\to tZ'}\left(\alpha_s(\sqrt{s}/\tilde{N}')\right) \\
&\quad \times \exp\left[2\int_{\sqrt{s}}^{\sqrt{s}/\tilde{N}'}\frac{d\mu}{\mu}\,\Gamma^S_{gq\to tZ'}(\alpha_s(\mu))\right]. \qquad (3.5)
\end{aligned}
$$

Soft-gluon resummation is the exponentiation of logarithms of N. The first exponent in Eq. (3.5) includes soft and collinear corrections [46,47] from the incoming partons, and can be found explicitly in [35–39].

We write the perturbative series for the soft anomalous dimension for $gq \to tZ'$ as $\Gamma^S_{gq\to tZ'} = \sum_{n=1}^{\infty}(\alpha_s/\pi)^n \Gamma^{S(n)}_{gq\to tZ'}$. To achieve resummation at next-to-leading-logarithm (NLL) accuracy we require the one-loop result which

is given, in Feynman gauge, by

$$\Gamma^{S\,(1)}_{gq\to tZ} = C_F\left[\ln\left(\frac{-u_1}{m_t\sqrt{s}}\right)-\frac{1}{2}\right]+\frac{C_A}{2}\ln\left(\frac{t_1}{u_1}\right), \quad (3.6)$$

with color factors $C_F = (N_c^2-1)/(2N_c)$ and $C_A = N_c$, where $N_c = 3$ is the number of colors.

Upon expanding the resummed cross section to fixed order and inverting from the transform moment space back to momentum space, the logarithms of N produce "plus" distributions of logarithms of $s_4/m^2_{Z'}$. The highest power of these logarithms is 1 at NLO and 3 at NNLO.

The NLO soft-gluon corrections for $gq \to tZ'$ are

$$\begin{aligned}\frac{d^2\hat{\sigma}^{(1)}_{gq\to tZ'}}{dt\,du} &= F^{\rm LO}_{gq\to tZ'}\frac{\alpha_s(\mu_R^2)}{\pi}\left\{2(C_F+C_A)\left[\frac{\ln(s_4/m^2_{Z'})}{s_4}\right]_+\right.\\ &+\left[2C_F\ln\left(\frac{u_1}{t_2}\right)+C_F\ln\left(\frac{m^2_{Z'}}{m_t^2}\right)\right.\\ &-C_F+C_A\ln\left(\frac{t_1}{u_1}\right)+C_A\ln\left(\frac{sm^2_{Z'}}{u_2^2}\right)\\ &\left.-(C_F+C_A)\ln\left(\frac{\mu_F^2}{m^2_{Z'}}\right)\right]\left[\frac{1}{s_4}\right]_+\\ &+\left[\left(C_F\ln\left(\frac{-t_2}{m^2_{Z'}}\right)+C_A\ln\left(\frac{-u_2}{m^2_{Z'}}\right)\right.\right.\\ &\left.\left.-\frac{3}{4}C_F\right)\ln\left(\frac{\mu_F^2}{m^2_{Z'}}\right)-\frac{\beta_0}{4}\ln\left(\frac{\mu_F^2}{\mu_R^2}\right)\right]\delta(s_4)\Bigg\},\end{aligned} \quad (3.7)$$

where $\beta_0 = (11C_A - 2n_f)/3$ is the lowest-order QCD β function, with n_f the number of light quark flavors. We set $n_f = 5$ for $gu \to tZ'$ and $gc \to tZ'$, and $n_f = 6$ for $gt \to tZ'$. The leading logarithms in the NLO expansion are the $[\ln(s_4/m^2_{Z'})/s_4]_+$ terms while the NLL are the $[1/s_4]_+$ terms. In addition, at NLL we determine in Eq. (3.7) the $\delta(s_4)$ terms involving the scale. In top-quark production processes, the NLO soft-gluon corrections approximate very well the complete NLO corrections [30–40]. We denote the sum of the LO cross section and the NLO soft-gluon corrections as approximate NLO (aNLO).

The NNLO soft-gluon corrections for $gq \to tZ'$ are

$$\begin{aligned}&\frac{d^2\hat{\sigma}^{(2)}_{gq\to tZ'}}{dt\,du}\\ &= F^{\rm LO}_{gq\to tZ'}\frac{\alpha_s^2(\mu_R^2)}{\pi^2}\left\{2(C_F+C_A)^2\left[\frac{\ln^3(s_4/m^2_{Z'})}{s_4}\right]_+\right.\\ &+3(C_F+C_A)\left[2C_F\ln\left(\frac{u_1}{t_2}\right)+C_F\ln\left(\frac{m^2_{Z'}}{m_t^2}\right)\right.\\ &-C_F+C_A\ln\left(\frac{t_1}{u_1}\right)+C_A\ln\left(\frac{sm^2_{Z'}}{u_2^2}\right)\\ &-(C_F+C_A)\ln\left(\frac{\mu_F^2}{m^2_{Z'}}\right)-\frac{\beta_0}{6}\Bigg]\left[\frac{\ln^2(s_4/m^2_{Z'})}{s_4}\right]_+\\ &+2(C_F+C_A)\left[\left(3C_F\ln\left(\frac{-t_2}{m^2_{Z'}}\right)-2C_F\ln\left(\frac{-u_1}{m^2_{Z'}}\right)\right.\right.\\ &-C_F\ln\left(\frac{m^2_{Z'}}{m_t^2}\right)+\frac{C_F}{4}+3C_A\ln\left(\frac{-u_2}{m^2_{Z'}}\right)\\ &+C_A\ln\left(\frac{u_1m^2_{Z'}}{t_1s}\right)-\frac{\beta_0}{4}\Bigg)\ln\left(\frac{\mu_F^2}{m^2_{Z'}}\right)+\frac{\beta_0}{2}\ln\left(\frac{\mu_R^2}{m^2_{Z'}}\right)\\ &+\frac{1}{2}(C_F+C_A)\ln^2\left(\frac{\mu_F^2}{m^2_{Z'}}\right)\\ &\left.-2(C_F+C_A)\zeta_2\Bigg]\left[\frac{\ln(s_4/m^2_{Z'})}{s_4}\right]_+\right.\\ &+(C_F+C_A)\left[\left(\frac{3\beta_0}{8}+\frac{3}{4}C_F-C_F\ln\left(\frac{-t_2}{m^2_{Z'}}\right)\right.\right.\\ &\left.\left.-C_A\ln\left(\frac{-u_2}{m^2_{Z'}}\right)\right)\ln^2\left(\frac{\mu_F^2}{m^2_{Z'}}\right)\right.\\ &-\frac{\beta_0}{2}\ln\left(\frac{\mu_F^2}{m^2_{Z'}}\right)\ln\left(\frac{\mu_R^2}{m^2_{Z'}}\right)\\ &-2\zeta_2\left(2C_F\ln\left(\frac{u_1}{t_2}\right)+C_F\ln\left(\frac{m^2_{Z'}}{m_t^2}\right)\right.\\ &-C_F+C_A\ln\left(\frac{t_1}{u_1}\right)+C_A\ln\left(\frac{sm^2_{Z'}}{u_2^2}\right)\\ &\left.\left.-(C_F+C_A)\ln\left(\frac{\mu_F^2}{m^2_{Z'}}\right)\right)\right.\\ &\left.+4(C_F+C_A)\zeta_3\Bigg]\left[\frac{1}{s_4}\right]_+\right\}. \end{aligned} \quad (3.8)$$

The leading logarithms in the NNLO expansion are the $[\ln^3(s_4/m^2_{Z'})/s_4]_+$ terms while the NLL are the $[\ln^2(s_4/m^2_{Z'})/s_4]_+$ terms. Moreover, at NLL we determine in Eq. (3.8) additional terms involving the scale. The cross section with the inclusion of the soft-gluon corrections through NNLO is denoted as approximate NNLO (aNNLO).

4 Phenomenological analysis

In the following sections we present the results of our phenomenological analysis in which we investigate the impact of the QCD corrections due to soft gluon emissions to the production of a single top quark in association with a Z' for the case studies previously discussed.

According to recent LHC Run II exclusion limits [48,49], extra neutral currents with masses $m_{Z'} \lesssim 4$ TeV are disfavoured. In our analysis we consider final-state Z's with masses ranging from 1 to 8 TeV where lighter Z' masses are still included, because we wish to illustrate the behavior of the cross section and its scaling with the different phase-space suppression due to a final state with Z' masses from low to high.

4.1 Comparison with existing results at NLO

We first illustrate a comparison of our aNLO calculation against other existing results at NLO. Then we discuss the matching of our aNNLO calculation to the exact NLO at fixed order in QCD. To validate the formalism at aNLO, we use tZ production at the LHC in the presence of FCNC and compare the total cross section and scale dependence for the $gu \to tZ$ channel at NLO to the results of Ref. [50]. The comparison is summarized in Table 1 and was already documented in Ref. [30].

These numbers are in very good agreement (within 2 per mille) with Ref. [50] and can be checked in Table 1 and Fig. 6 respectively in that paper. They show that the soft-gluon approximation is excellent for these processes. As also noted in Ref. [30], the agreement between aNLO and NLO is also very good for the $gc \to tZ$ channel.

A second independent cross check for the $gu \to tZ$ channel was made by using MadGraph5_aMC@NLO [52] which provides both the total rate and the top-quark p_T distribution. We have used the FCNC Madgraph module described in Refs. [53,54] which employs a general approach to top-quark FCNC based on effective field theory. We fixed the parameters such that we could compare the cross section relative to the tensor interaction term only in the Lagrangian. We obtained the results illustrated in Fig. 3 where the aNLO prediction is in very good agreement with the NLO calculation.

In the case of tZ' production, our aNLO results have also been compared to the full NLO calculation at 7 TeV LHC energy provided in Ref. [15]. In particular, we compared K-factors. It is important to notice that the Lagrangian used to obtain the results in Ref. [15] only includes vector interaction contributions, e.g., $\mathcal{L}_{Z'} = (Q_{tU}/\sqrt{2})\bar{U}\gamma^\mu g_R P_R t Z'_\mu + h.c.$, where Q_{tU} is a coupling factor, g_R is a coupling constant, P_R is the right-handed chiral projector, and U denote the generic up-type quark. In this study, we consider only tensor interactions (cf. Eq. (2.1)). Moreover, the authors of Ref. [15] have used different PDFs, MSTW2008 [55], and a different choice of central scale, $(m_{Z'} + m_t)/2$, than our choice of central scale, $m_{Z'}$. Therefore, to make a valid comparison between K-factors from vector and tensor interactions, we have adopted their PDFs and scale choices to make a comparison at 7 TeV. Because they use Run 1 LHC energies, the authors of Ref. [15] only show results up to $m_{Z'}$ masses of 2000 GeV. In Fig. 4 we display NLO/LO K-factors relative to vector interactions and aNLO/LO K-factors relative to tensor interactions for $\mu = (m_{Z'} + m_t)/2$, and a variation of that scale by a factor of two up and down for the NLO and aNLO corrections at these scales relative to the central LO result at $\mu = (m_{Z'} + m_t)/2$. We find that tensor interactions give K-factors at aNLO which are very similar in magnitude to those obtained by using vector interactions, but the scale dependence for the tensorial case is found to be somewhat smaller than (but consistent with) the vector case. We stress, however, that we do not expect exact agreement between the two cases due to the different Lagrangians involved. In the inset plot of Fig. 4 we also display the additional enhancements from the aNNLO corrections, where in the numerator of aNNLO/aNLO we use NNLO PDFs and in the denominator we use NLO PDFs.

In conclusion, we have shown that for tZ production the soft-gluon corrections account for the overwhelming majority of the complete corrections and that the aNLO calculation is very trustworthy. This was already demonstrated for tZ production in Ref. [30] and it is also consistent with the fact that the NLO soft-gluon corrections approximate very well the complete NLO corrections for $t\gamma$ [31] production via anomalous couplings, as well as for top-pair [32–34] and single-top [35–39] production.

4.2 Matching to the NLO theory at fixed order in QCD

The formalism utilized in this study is expected to work equally well in the case of tZ' production, because it is essentially the same, the only difference being that the mass of the Z' can have different values. Indeed, after performing the aNLO and NLO calculations for tZ' production for a variety of collider energies and Z' masses, we observed that the aNLO and the exact NLO results differ by a few percent. As expected, at large collider energies and large $m_{Z'}$ values, soft-gluon corrections account for the overwhelming majority of the QCD corrections, and the difference between the approximate and the exact NLO predictions is found to be very small.

To further improve our theoretical predictions, we match our aNNLO prediction to the exact NLO theory at fixed order in QCD, and in the rest of this paper we show phenomenological results at NLO and aNNLO. The NLO fixed order theory prediction for both the FCNC and the stringy inspired tZ' production is obtained with MadGraph5_aMC@NLO-v2.7.2, which we have used to calculate both the total rate and the top-quark p_T distributions. The approximate aNNLO theory prediction is obtained by matching to the NLO as fol-

Table 1 Total rate comparison for $gu \to tZ$ at the LHC 14 TeV: aNLO vs NLO from Ref. [50]. The cross section σ_0 is the default central value obtained using the central scale choice $\mu = m_Z + m_t$, i.e. $\sigma_0 = \sigma(\mu = m_Z + m_t)$. The scale dependence is obtained by varying μ up and down by a factor of 2, i.e. $(m_Z+m_t)/2 \le \mu \le 2(m_Z+m_t)$. CTEQ6M NLO PDFs [51] are used

σ_0^{aNLO}	σ_0^{NLO} (Ref. [50])	$(\sigma(\mu)/\sigma_0)_{\text{aNLO}}$	$(\sigma(\mu)/\sigma_0)_{\text{NLO}}$ (Ref. [50])
22.55 pb	22.5 pb	0.912 $\mu=2(m_Z+m_t)$ 1.103 $\mu=(m_Z+m_t)/2$	0.913 $\mu=2(m_Z+m_t)$ 1.112 $\mu=(m_Z+m_t)/2$

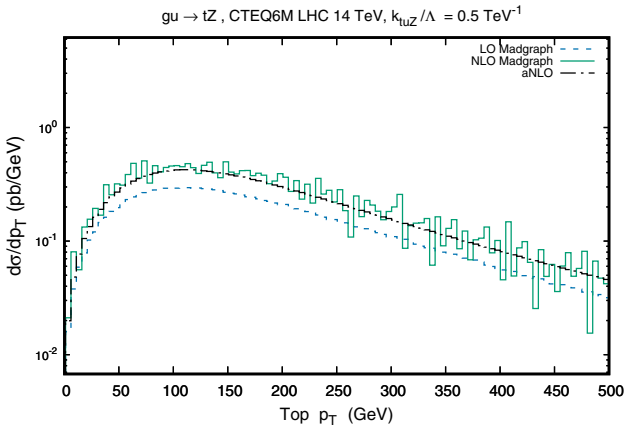

Fig. 3 aNLO vs NLO Madgraph top-quark p_T distribution at the 14 TeV LHC

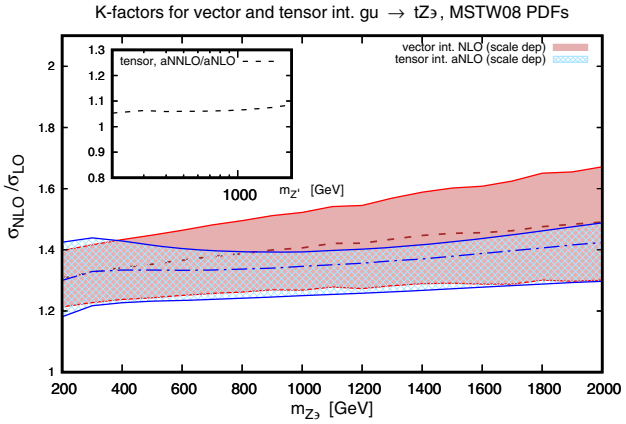

Fig. 4 NLO K-factors for top FCNC with vector interactions and the aNLO K-factors for top FCNC with tensor interactions for the $gu \to tZ'$ channel at the LHC at 7 TeV. Scale variation refers to $(m_{Z'} + m_t)/4 \le \mu \le m_{Z'} + m_t$. The inset plot also shows the aNNLO K-factors

lows:

$$\sigma_{aNNLO} = \left[\hat{\sigma}_{LO} + \hat{\sigma}_{NLO} + \hat{\sigma}_{aNNLO}\right]_{ij} \otimes f_i^{NNLO} \otimes f_j^{NNLO}, \tag{4.1}$$

where the soft-gluon contributions from the aNNLO hard scattering are added on top of the fixed-order NLO. The matching procedure ensures a better control of kinematic regions of the phase space where soft-gluons are less dominant.

4.3 FCNC Z's: $gu \to tZ'$ and $gc \to tZ'$

We first study tZ' production via FCNC interactions with anomalous couplings. The partonic processes involved are $gu \to tZ'$ and $gc \to tZ'$, where the Z' anomalously couples to the top quark and the u and c quarks through the flavor-changing coefficients $k_{tuZ'}/\Lambda$ and $k_{tcZ'}/\Lambda$, respectively. The scale Λ is set equal to ten times the top quark mass m_t and the couplings $k_{tuZ'}$ and $k_{tcZ'}$ are considered as parameters of the theory. As a case study we select $k_{tuZ'} = k_{tcZ'} = 0.1$. Thus, in our results below we set $k_{tuZ'}/\Lambda = k_{tcZ'}/\Lambda = 0.01/m_t$. We also set $m_t = 172.5$ GeV. Recent experimental searches for and phenomenological studies of FCNC interactions between the top quark and a Z boson can be found in Refs. [56–60].

We explore cross sections at 13 and 14 TeV LHC energies for a large range of Z' masses, and also explore the cross sections as functions of pp collider energy for future colliders. The theory predictions in this case are obtained by using the CT14 PDFs [61] which lead to the numerical results illustrated in Figs. 5, 6, 7, 8, 9, 10, 11, 12, 13, 14, 15 and 16. In this case, PDF induced uncertainties are calculated at the 68% confidence level (C.L.) (see Appendix A for a discussion on PDF uncertainties).

The initial-state parton combinations $g(x_1)u(x_2) + g(x_2)u(x_1)$ and $g(x_1)c(x_2) + g(x_2)c(x_1)$ are probed in various kinematic regions depending on the collider center-of-mass energy and on the mass of the Z'. At $\sqrt{S} = 13$ TeV and $1 \lesssim M_{Z'} \lesssim 8$ TeV, one probes large x values $x \ge 0.1$ where the current PDFs are not well constrained and their uncertainties are large. At higher collider energies $\sqrt{S} = 100$ TeV, one probes $10^{-4} \lesssim x \lesssim 0.1$ for $M_{Z'} \approx 1$ TeV, and $0.01 \lesssim x \lesssim 0.1$ for $M_{Z'} \approx 8$ TeV.

The total cross sections at collider energies of 13 TeV are illustrated in Fig. 5 where we show the theory predictions at LO, NLO, and aNNLO for the process $gu \to tZ'$ with anomalous $k_{tuZ'}$ coupling, and the process $gc \to tZ'$ with anomalous $k_{tcZ'}$ coupling, as functions of Z' mass. Here CT14NNLO PDFs are used for the LO, NLO, and aNNLO calculations to show soft-gluon enhancements in the hard-scattering contributions with respect to the Born cross section. The factorization and renormalization scales are equal and set to $\mu = m_{Z'}$. We observe a very strong dependence of

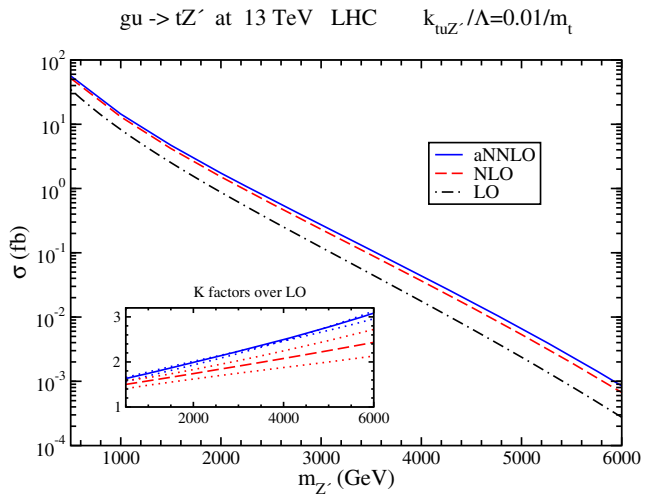

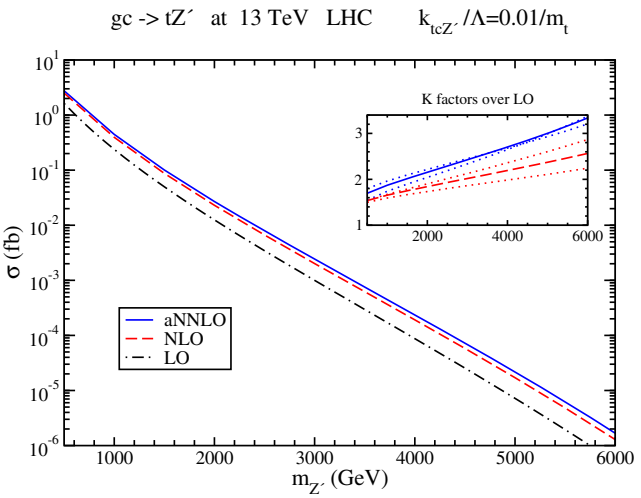

Fig. 5 Total cross sections at 13 TeV LHC energy for (left) $gu \to tZ'$ with anomalous t–u–Z' coupling and (right) $gc \to tZ'$ with anomalous t–c–Z' coupling. The inset plots display K-factors. Here CT14NNLO PDFs are used for the LO, NLO, and aNNLO calculations to show the enhancement due to hard-scattering contributions

the cross section on the Z' mass. The cross section drops over many orders of magnitude as the Z' mass varies from 1 TeV to 6 TeV. The cross section for $gc \to tZ'$ is significantly smaller than for $gu \to tZ'$. The inset plots show the NLO/LO and aNNLO/LO K-factors with scale uncertainty bands which are obtained by varying μ in the interval $[1/2\mu, 2\mu]$ in the numerator. The K-factors are large and increase with larger Z' masses, as expected. The NLO corrections are large and furthermore the additional aNNLO corrections are very significant. We also provide numerical values for the $gu \to tZ'$ cross section and K-factors in Table 2 of Appendix C.

The corresponding results at 14 TeV energy are shown in Fig. 6. The cross sections are of course larger than at 13 TeV, but the dependence on the Z' mass and the size of the corrections are very similar.

In Fig. 7 we show the total cross sections at NLO and aNNLO for the processes $gu \to tZ'$ and $gc \to tZ'$ at 13, 27, 50, and 100 TeV collider energies together with CT14 PDF uncertainties evaluated at the 68% confidence level (C.L.). In this case, the aNNLO total cross sections are obtained with CT14NNLO PDFs, while the NLO's are obtained with CT14NLO. The inset plots show the $\sigma_{aNNLO}/\sigma_{NLO}$ K-factors. We note that the $\sigma_{aNNLO}/\sigma_{LO}$ K-factors are not shown here because there are no CT14 PDFs at LO. We observe that the $\sigma_{aNNLO}/\sigma_{NLO}$ K-factors provide large corrections for large values of $m_{Z'}$, and the corrections decrease as the collider energy increases. The induced PDF uncertainty of both gu and gc channels is larger at lower collider energy and high $m_{Z'}$ where PDFs are weakly constrained.

Figure 8 shows total cross section predictions at 13, 27, 50, and 100 TeV collider energies using CT14NNLO PDFs at all orders for FCNC tZ' production to show the enhancement due to soft gluons in the perturbative series.

The behavior of the cross section with collider energy is illustrated in Fig. 9, where we show results at LO, NLO, and aNNLO for the gu and gc channels as functions of the collider energy up to 100 TeV for three choices of Z' mass, $m_{Z'} = 3$, 5, and 8 TeV. Here, the LO, NLO, and aNNLO cross sections are obtained with CT14NNLO PDFs to show enhancement in the hard scattering due to soft gluon corrections. The cross sections are smaller for larger Z' masses due to phase-space suppression. The inset plots show the NLO/LO and aNNLO/LO K-factors. As expected, the K-factors are larger at smaller energies and also for higher Z' masses, since we are then closer to threshold.

In the case of tZ' production with FCNC couplings, the anomalous couplings entering both channels of the cross section are considered as free parameters. We have therefore performed a two dimensional scan to assess the sensitivity of the cross section. In Fig. 10 we show a case study in which we plot aNNLO total cross sections as functions of the couplings $k_{tuZ'}/\Lambda$ and $k_{tcZ'}/\Lambda$, at a collider energies of 13 and 100 TeV, for different values of $m_{Z'}$. We notice that if we let both couplings to vary in $10^{-5} \leq k/\Lambda \leq 0.1$ TeV^{-1}, the cross section spans several orders of magnitude. The cross section suppression is larger for larger values of $m_{Z'}$.

4.3.1 *Top-quark p_T distributions for FCNC $Z's$*

It is interesting to study kinematic distributions such as the top-quark p_T differential distribution, $d\sigma/dp_T$, and how $Z's$ of different masses affect the p_T suppression in various kinematic ranges. We illustrate the top-quark p_T distribu-

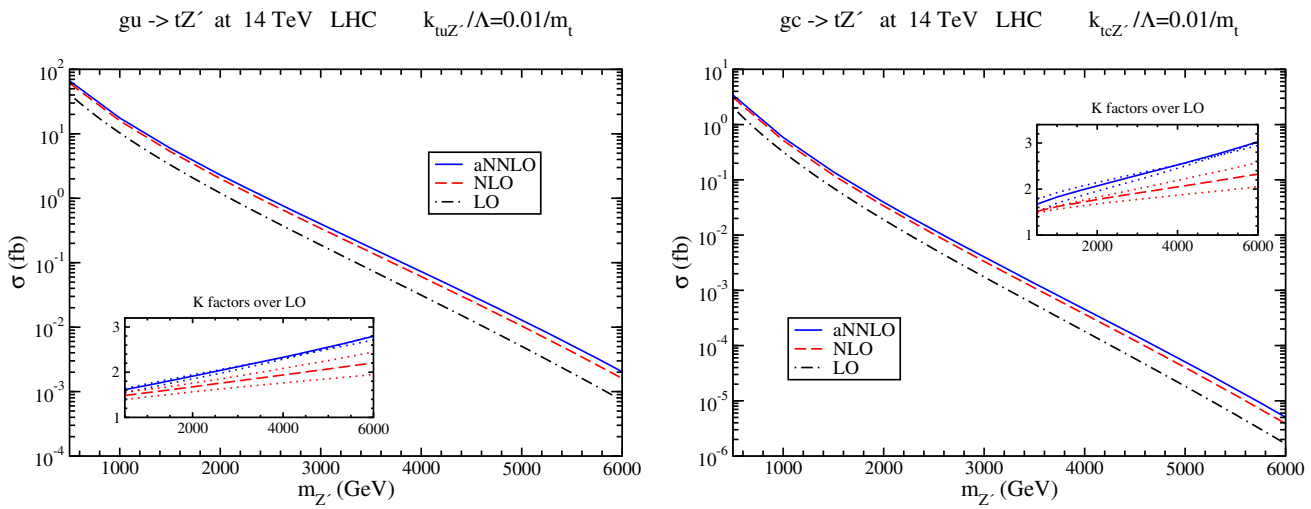

Fig. 6 Total cross sections at 14 TeV LHC energy for the (left) $gu \to tZ'$ and (right) $gc \to tZ'$ processes with anomalous couplings. The inset plots display K-factors. Here CT14NNLO PDFs are used for the LO, NLO, and aNNLO calculations to show the enhancement due to hard-scattering contributions

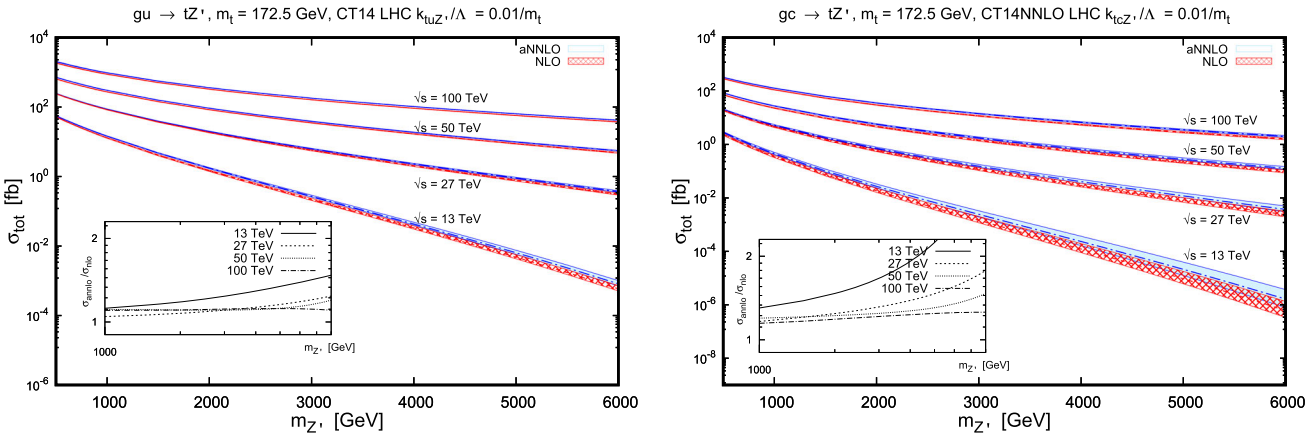

Fig. 7 Total cross sections for the (left) $gu \to tZ'$ and (right) $gc \to tZ'$ processes with anomalous couplings. The plots show results including CT14 PDF uncertainties for several center-of-mass energies of the pp collision as a function of Z' mass. The aNNLO cross section is obtained with CT14NNLO PDFs while the NLO with CT14NLO. The CT14 PDF uncertainties are at the 68% C.L. The inset plots show the $\sigma_{aNNLO}/\sigma_{NLO}$ K-factors

tions, calculated by a numerical integration of the double-differential distribution, in Fig. 11. Results for the $gu \to tZ'$ and $gc \to tZ'$ processes at a collider energy of 100 TeV are shown at LO, NLO, and aNNLO, obtained with CT14NNLO PDFs, for three choices of the Z' mass of 3, 5, and 8 TeV.

The NLO corrections are large and furthermore the additional aNNLO corrections are important. The p_T distributions decrease quickly as $m_{Z'}$ is increased, but they are non-negligible even for large Z' masses, indicating that the number of events predicted by these models can be validated at the high-luminosity FCC or SppC colliders. The K-factors, shown in the inset plots, are significant and their value depends on $m_{Z'}$ and on the phase-space supression.

4.3.2 *Cross section and PDF correlations*

Next, we explore the extent of correlation between the PDFs and the aNNLO cross section for these processes in pp collisions at $\sqrt{S}$=13 and 100 TeV. PDF correlations are important because they give us information about the kinematic region in which PDFs are probed and for example, they give us indication of the impact of the gluon at different values of the momentum fraction x. In order to set tighter constraints on Z's models it is important to understand how PDF uncertainties come into play and how to improve their precision through dedicated QCD global analyses.

In particular, in Fig. 12 we show the correlation cosine between the gluon (and the u quark) and the total cross sec-

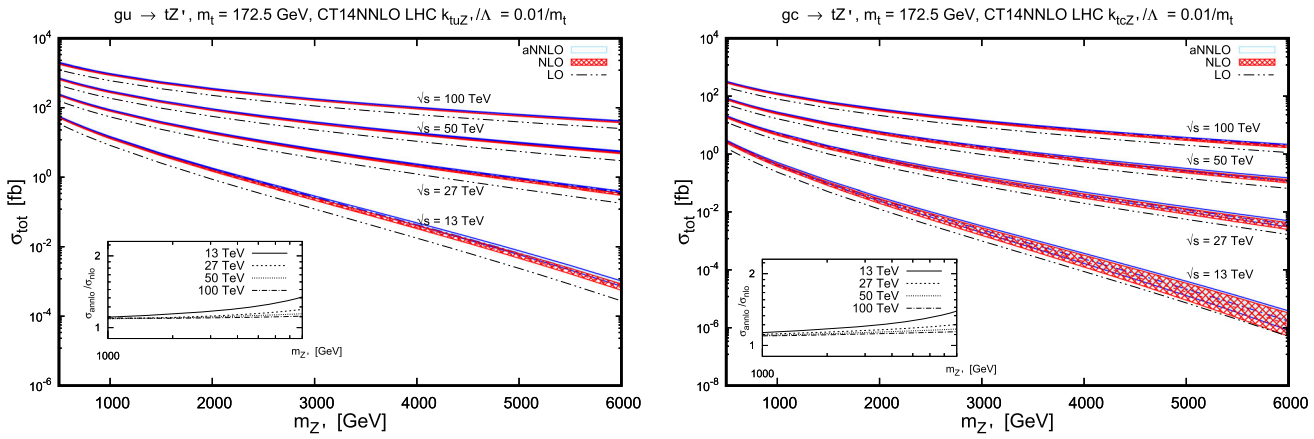

Fig. 8 Total cross sections for the $gu \to tZ'$ (left) and the $gc \to tZ'$ (right) processes with anomalous couplings. The plots show results with CT14 NNLO PDF uncertainties at 68% C.L. for several center-of-mass energies of the pp collision as a function of $m_{Z'}$

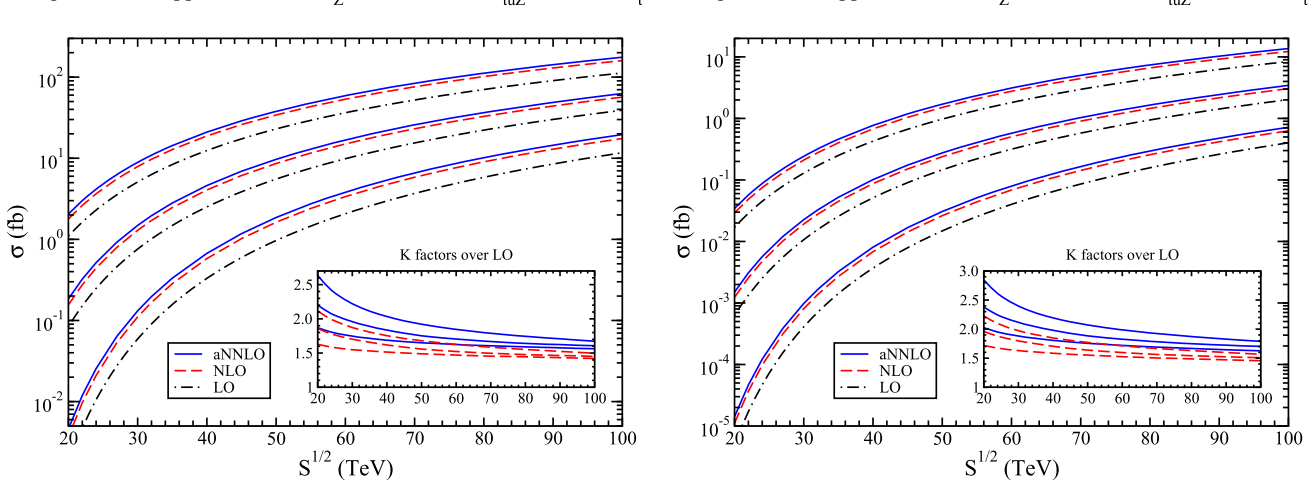

Fig. 9 Total cross sections for the (left) $gu \to tZ'$ and (right) $gc \to tZ'$ processes with anomalous couplings. The plots show results as a function of collider energy for three choices of Z' mass, 3, 5, and 8 TeV. The inset plots display K-factors. CT14NNLO PDFs are used

tion for the $gu \to tZ'$ process as a function of the momentum fraction x at the 68% CL at $\sqrt{S} = 13$ and 100 TeV. We have chosen the gu channel as it provides the dominant contribution. The definition of the correlation cosine between two quantities determined within the Hessian method is given in Appendix B. At collider energies of 13 TeV, we observe a strong correlation ($\cos\phi \geq 0.8$) between the gluon and the $gu \to tZ'$ cross section at large $x \geq 0.1$ as expected, and the correlation peak shifts towards larger x values for larger $m_{Z'}$. Anti-correlation of approximately 50% in the $10^{-4} \leq x \leq 10^{-2}$ interval is also observed. The correlation between the u quark and the cross section is much milder and less than 50% at very large x. These patterns change as we move to higher collider energies, where for the gluon the correlation peak for each value of $m_{Z'}$ is shifted to lower x-values, while for the u quark correlations are slightly more pronounced.

Besides the correlation with PDFs, important information can also be gathered from the study of simultaneous uncertainty boundaries of the cross section of the gu and gc channels. The allowed regions are represented by correlation ellipses which can be compared to pseudo data in BSM simulations and explore the implications of the PDFs for this process. In Figs. 13 and 14 we show the elliptical confidence regions, at 68% CL, in pp collisions at 13 and 100 TeV, for $m_{Z'} = 1$, 3, 5, and 8 TeV. These can be used to read off PDF uncertainties and correlations for each pair of cross sections. At $\sqrt{S} = 13$ TeV, we notice that the two channels are highly correlated and the induced PDF uncertainties on the σ_{gc} channel are very large for this choice of the collider energy. This is reflected by the fact that there is a small portion of the ellipse where the PDF induced errors on the cross sections are larger than the cross section central value itself, allowing for negative values. At $\sqrt{S} = 100$ TeV, the gu

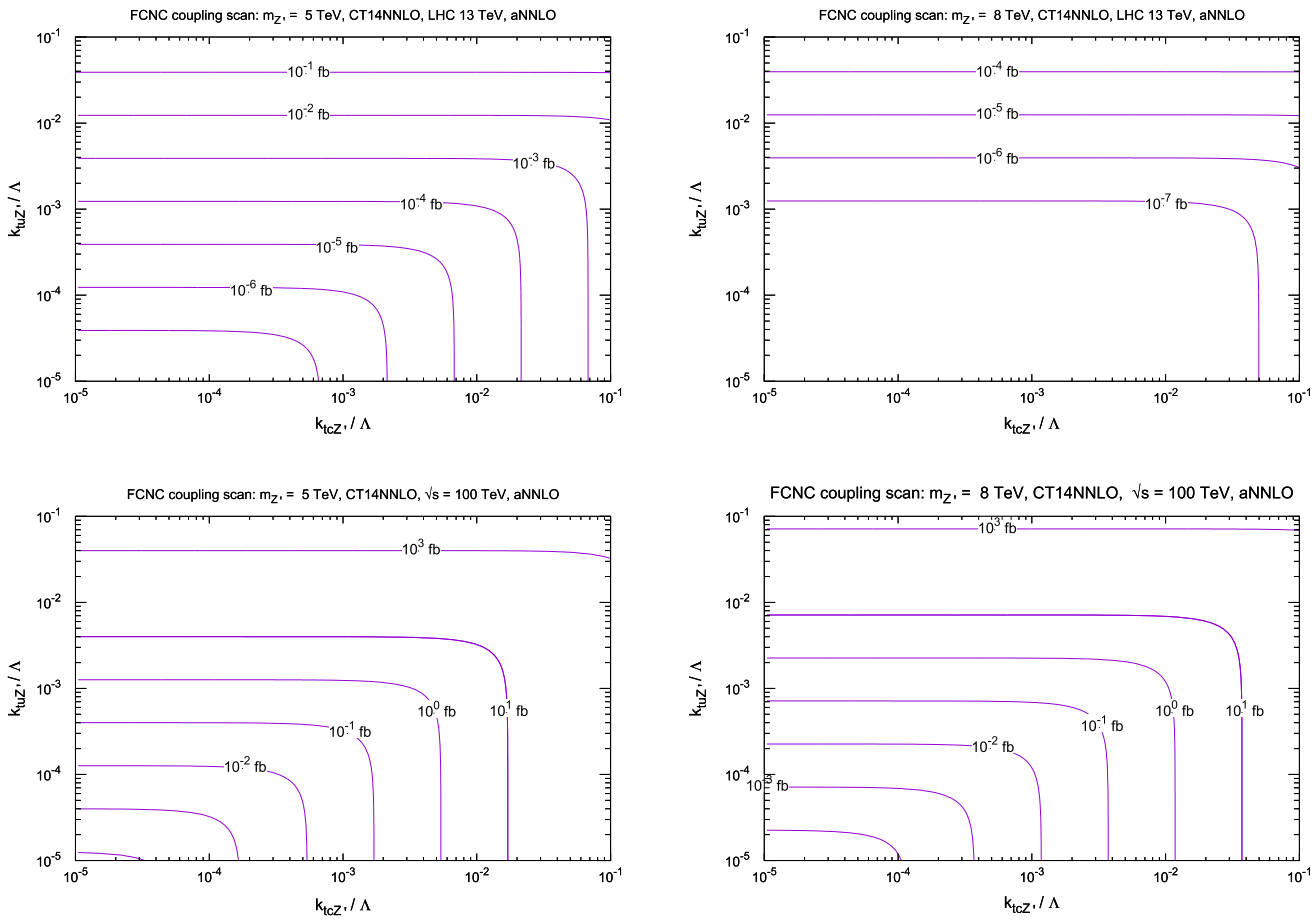

Fig. 10 Total cross sections for the $(gc + gu) \to tZ'$ process in a 2D contour plot. The insets show aNNLO results as a function of the anomalous couplings $k_{tuZ'}/\Lambda$ and $k_{tcZ'}/\Lambda$ (given in units of inverse m_t), in pp collisions at $\sqrt{S}$=13 and 100 TeV. CT14NNLO PDFs are used

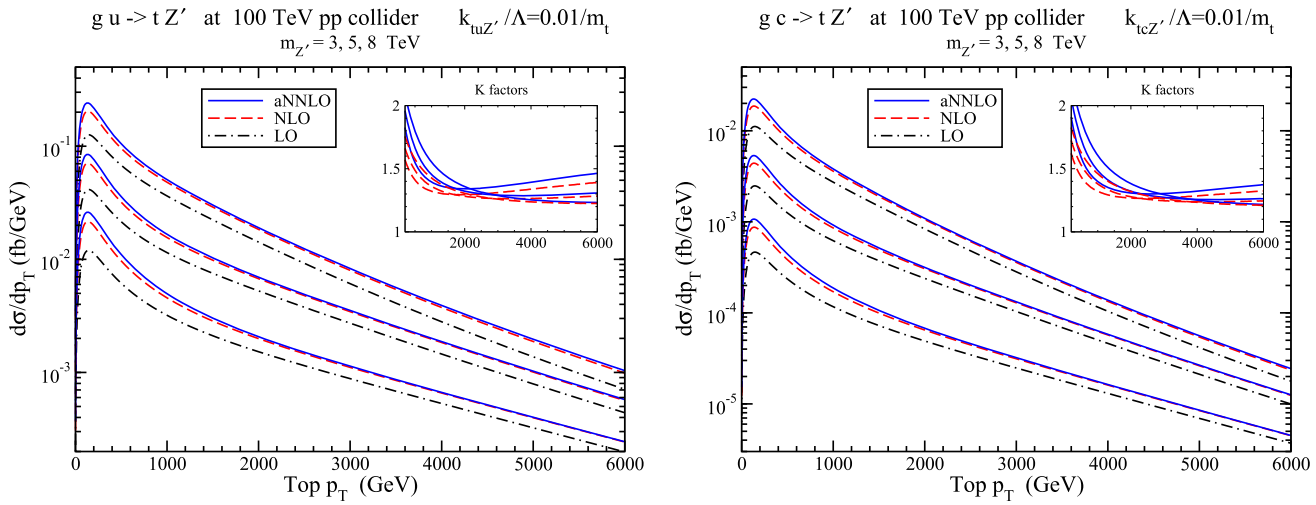

Fig. 11 Top-quark p_T distributions for the (left) $gu \to tZ'$ and (right) $gc \to tZ'$ processes with anomalous couplings for $m_{Z'} = 3$, 5, and 8 TeV at 100 TeV pp collider energy. Inset plots: NLO/LO and aNNLO/LO K-factors. CT14NNLO PDFs are used

and gc channels are still highly correlated, but the induced PDF uncertainties on both the cross sections are smaller as in this kinematic domain the PDFs are probed at intermediate x where they are better constrained.

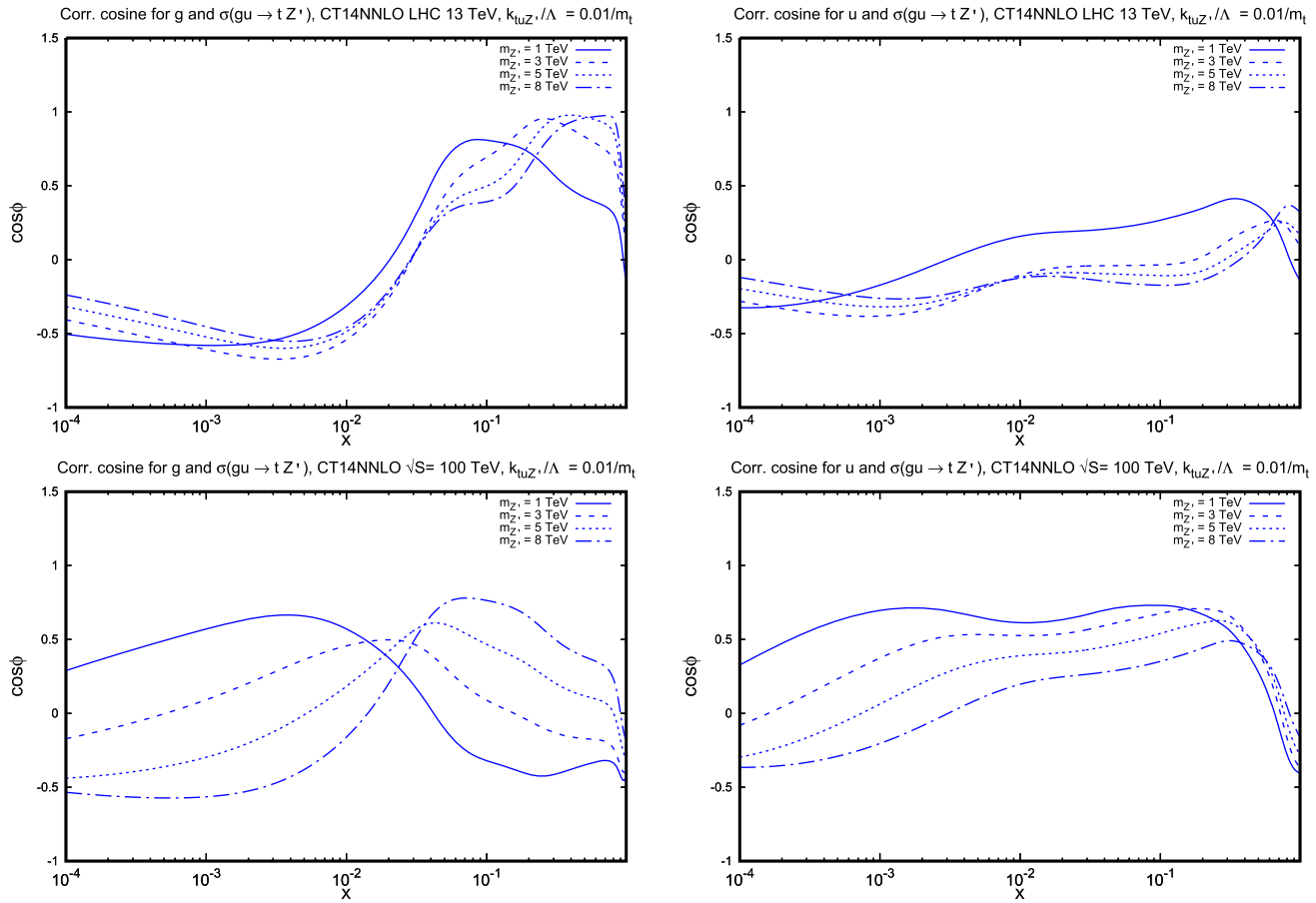

Fig. 12 Correlation cosine at $\sqrt{S}$=13 and 100 TeV between $\sigma_{gu\to tZ'}$ and the gluon as a function of x_{gluon} (left column) and $\sigma_{gu\to tZ'}$ and the up-quark as a function of x_{up} (right column). The four panels show aNNLO results rescaled at the 68% C.L. for different values of the Z' mass

Next, we study the impact of the scale and PDF uncertainties on the aNNLO/LO K-factors as functions of the collider energy for large $\sqrt{S}$ values and different values of $m_{Z'}$. In Figs. 15 and 16, we illustrate the K-factors for the gu and gc channels with CT14NNLO PDF and scale uncertainties respectively. Scale variation refers to $m_{Z'}/2 \leq \mu \leq 2m_{Z'}$ as before. In Fig. 15 the PDF uncertainties for each $m_{Z'}$ value are shown using bands with different hatches and color. At collider energies below 20 TeV PDF uncertainties are large because PDFs are probed in the large-x region. In the gc channel, PDF uncertainties are dominant because the charm-quark PDF is less constrained with respect to the gluon and u-quark. In Fig. 16 the scale dependence in the aNNLO K-factors for the gu and gc channels is illustrated separately.

4.4 String-inspired Z's: $gt \to tZ'$

In this section we discuss the phenomenological results obtained from the study of tZ' production where the Z' originates from a low-energy realization of string-inspired models. The interaction Lagrangian in Sect. 2.2, and the choice of the parameters we have examined, are based on the models published in Refs. [41,42]. These models have not been searched for by the ATLAS and CMS collaborations to the best of our knowledge, therefore the current limits on the Z' mass and couplings should in principle not be applied here. The Z' models described in Refs. [41,42] allow for non-sequential solutions (i.e. charge assignments which are not proportional to the hypercharge) that are phenomenologically interesting and could in principle be considered in future analyses by both ATLAS and CMS.

An accurate determination of the $gt \to tZ'$ cross section can play an important role to set constraints on the couplings of Z' to the fermion sector. In fact, this process can in principle be used together with Z' production in Drell–Yan to remove the degeneracy between quark and lepton couplings [62,63].

The leading-order cross section is given by the s- and t-channels of the $gt \to tZ'$ process and the structure of the couplings is given in Sect. 2.2. The $gt \to tZ'$ process with $m_{Z'}$ in the TeV range requires the top-quark PDF in the initial state. In our phenomenological application, $\mu = m_{Z'} \gg m_t$ and we consider the top quark as an active flavor inside the proton with very good approximation. Therefore, in the rest

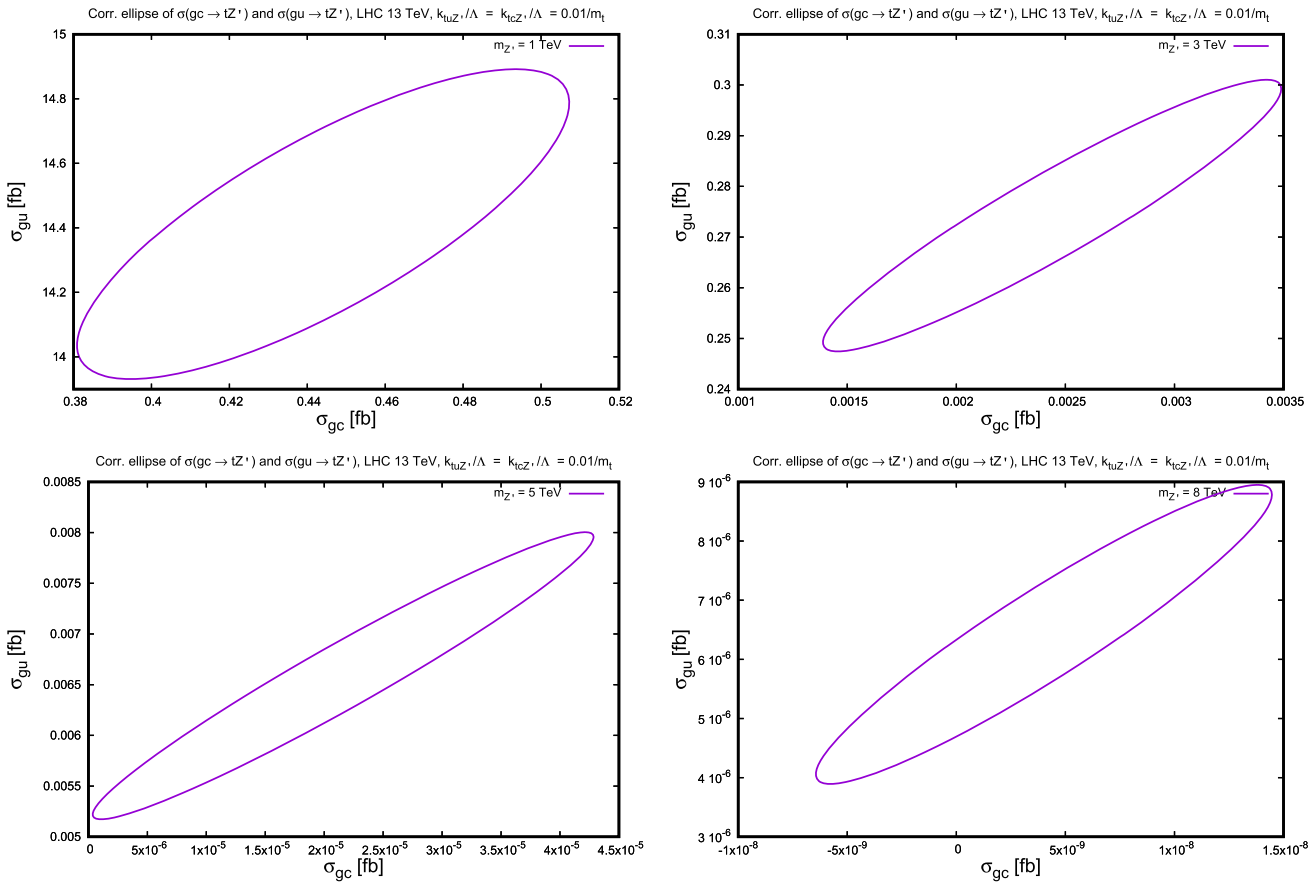

Fig. 13 Correlation ellipses of the $gu \to tZ'$ and $gc \to tZ'$ channels at $\sqrt{S} = 13$ TeV. The figures show CT14NNLO PDF induced uncertainty boundaries of the aNNLO results. Uncertainties are rescaled at the 68% C.L. for different values of the Z' mass

of this analysis we work with the 6-flavor scheme and use the NNPDF3.1 PDFs [64] with $n_f = 6$ and $\alpha_s(m_Z) = 0.118$, where n_f is the number of active flavors. We set $m_t = 0$ in the initial state lines in the calculation of the LO cross section. In this case, PDF uncertainties are calculated at 1-σ C.L. (see Appendix A) which is almost identical to the 68% C.L. in absence of statistical fluctuations in the determination of the PDFs.

In Fig. 17 we illustrate the top-quark PDF uncertainty as a function of x for different values of the final-state Z' mass. The $gt \to tZ'$ process probes the top-quark and gluon PDFs at large x where uncertainties are large at the LHC Run II collision energies. Precision measurements in the extended kinematic domain of the future FCC-eh collider will allow us to extract PDFs at large x for the individual quark flavors at the percent level precision. The precision of the top-quark PDF will be improved in this kinematic region enhancing the FCC-hh discovery potential of Z's with mass of $\mathcal{O}(10)$ TeV also in rare processes.

The left plot of Fig. 18 shows the NLO and aNNLO total cross section for the $gt \to tZ'$ process as a function of $m_{Z'}$ at collider energies $\sqrt{S} = 13, 27, 50, 100$ TeV. The error bands represent the induced PDF uncertainties on the cross section at 1-σ C.L. obtained by using NNPDF3.1 $n_f = 6$ PDFs. The aNNLO prediction is obtained using NNPDF3.1 NNLO $n_f = 6$ PDFs, while the NLO is obtained using NNPDF3.1 NLO $n_f = 6$ PDFs. The LO cross section is not shown here because the NNPDF3.1 $n_f = 6$ PDFs at LO are not available. The inset plot shows the $\sigma_{aNNLO}/\sigma_{NLO}$ K-factors from where we observe that the K-factors are large and they increase as $m_{Z'}$ increases, and they decrease when the collider energy increases, as for the case of the FCNC Z's.

In the plot on the right of Fig. 18, the cross section is obtained by convoluting hard scatterings at LO, NLO, and aNNLO, with NNLO PDFs in order to show the enhancement due to the hard-scattering contributions only.

The Z' coupling $g_{Z'}$ is considered as a free parameter and as a case study we choose $g_{Z'} = 1$ as the default choice. A $g_{Z'}$ parameter scan is illustrated in Fig. 19 (left) where the aNNLO cross section is plotted as a function of $\sqrt{S}$ for different values of $m_{Z'}$ which correspond to bands with different dashing. We explore $g_{Z'}$ variations in $0.01 \leq g_{Z'} \leq 1.5$ and observe that when $g_{Z'}$ varies the cross section is basically

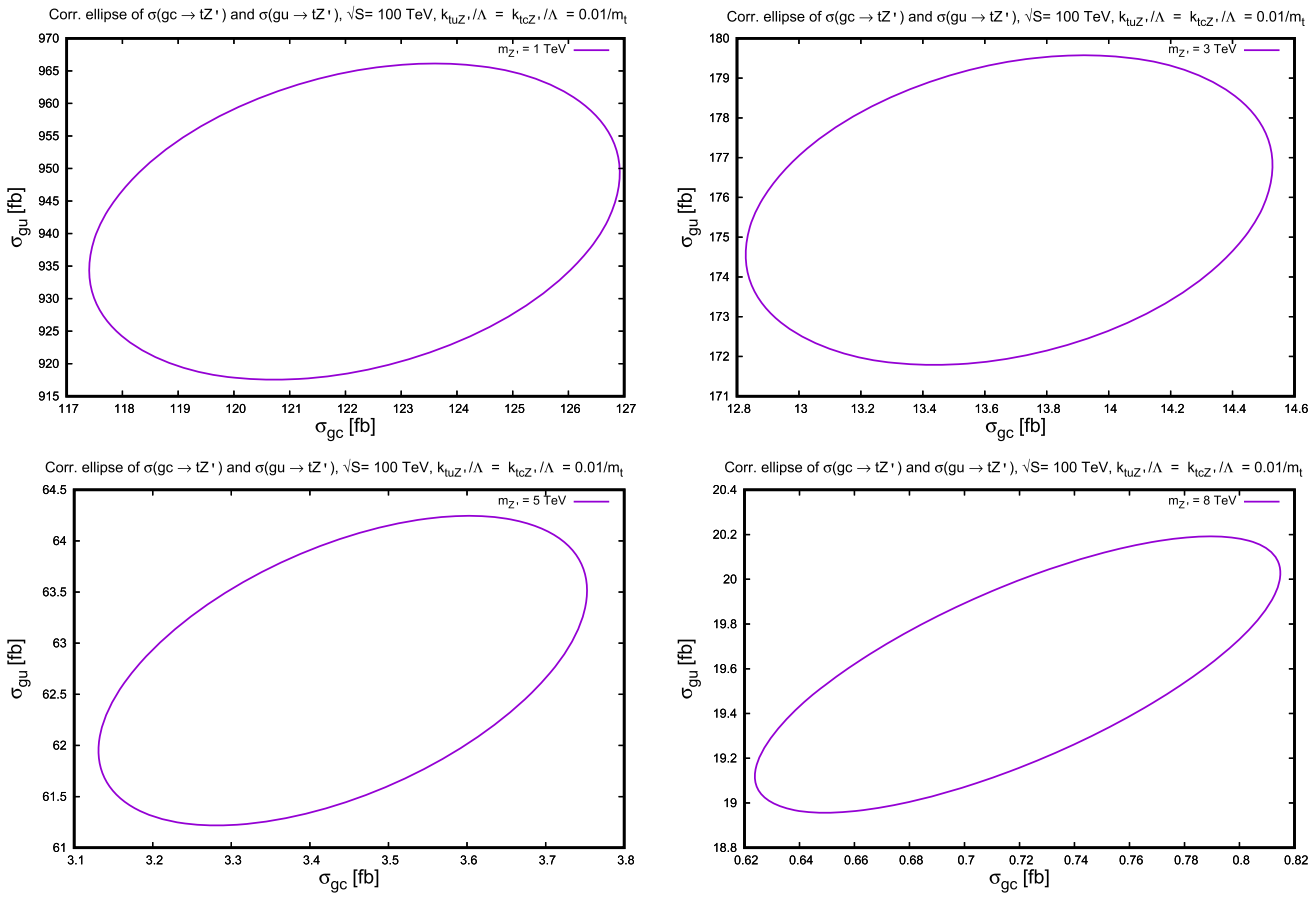

Fig. 14 Same as in Fig. 13, but for pp collisions at $\sqrt{S} = 100$ TeV

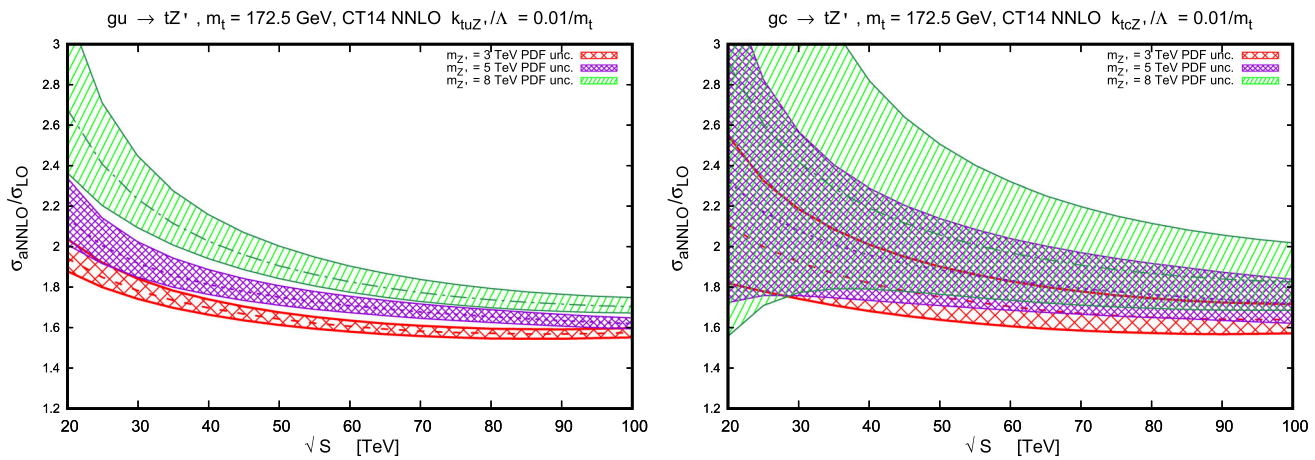

Fig. 15 K-factors with CT14NNLO PDF uncertainties (68% C.L.) for the $gu \to tZ'$ and $gc \to tZ'$ channels. The figures show a scan in the center of mass energy of the collisions $\sqrt{S}$ for different values of the Z' mass

rescaled and it spans approximately two orders of magnitude.

Moreover, for comparison purposes, we consider the production of a sequential Z' as a commonly-used point of reference. In Fig. 19 (right) we illustrate a comparison between aNNLO total cross sections for the production of string-inspired Z's and the production of sequential Z's, for different values of the collider energy. The sequential Z's are extra neutral vector bosons which have vector and axial-vector couplings equal to those of the SM Z-boson, but such that their right-handed and left-handed couplings to quarks are defined up to a constant factor which we set equal to

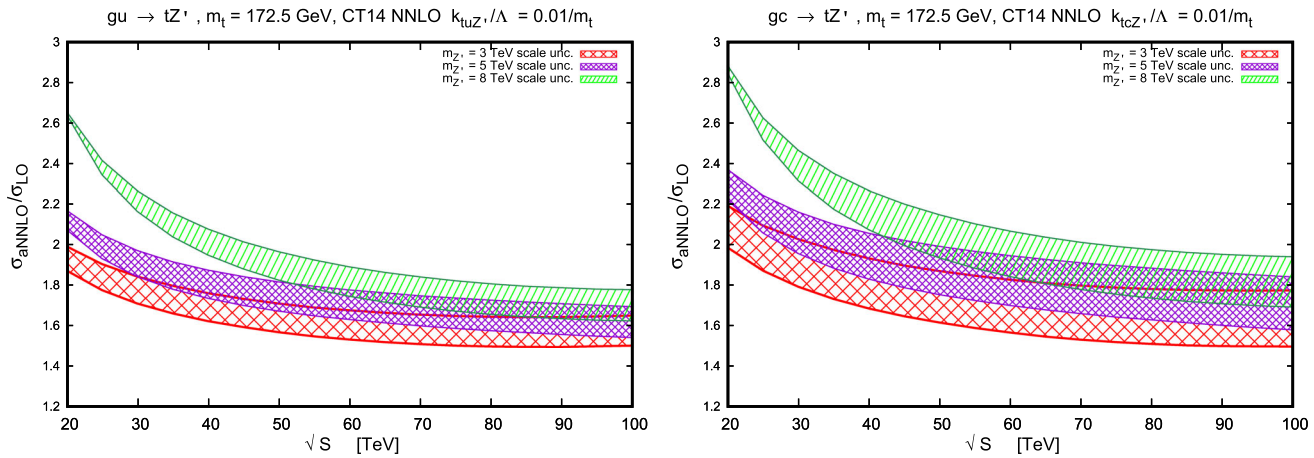

Fig. 16 Scale uncertainty in the aNNLO K-factors for the $gu \to tZ'$ and $gc \to tZ'$ channels. The figures show a scan in the center of mass energy of the collisions $\sqrt{S}$ for different values of the Z' mass. Scale variation refers to $m_{Z'}/2 \leq \mu \leq 2m_{Z'}$. CT14NNLO PDFs are used

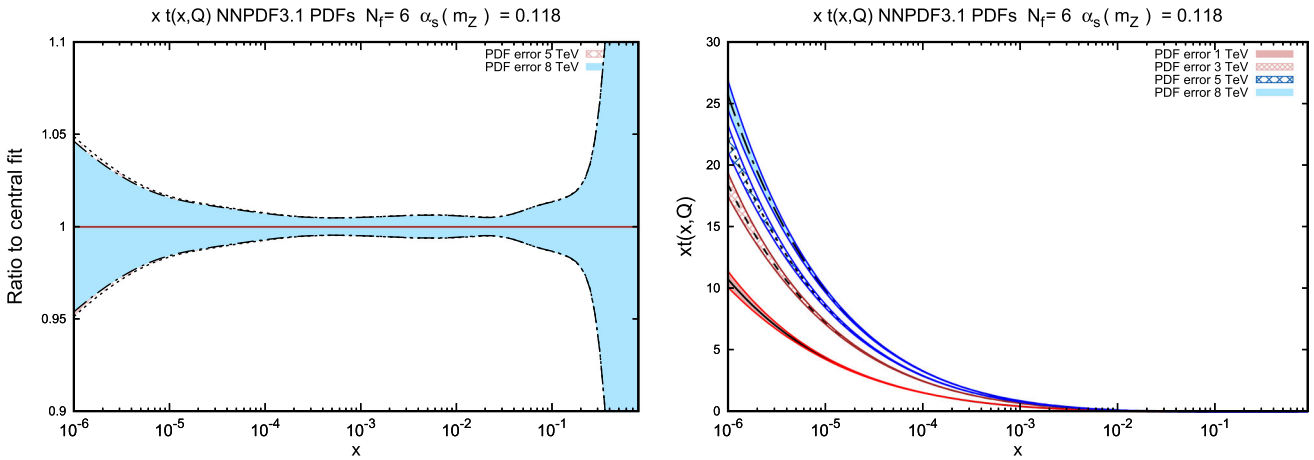

Fig. 17 The error bands represent NNPDF3.1 NNLO $n_f = 6$ PDF uncertainties evaluated at the 1-σ C.L.

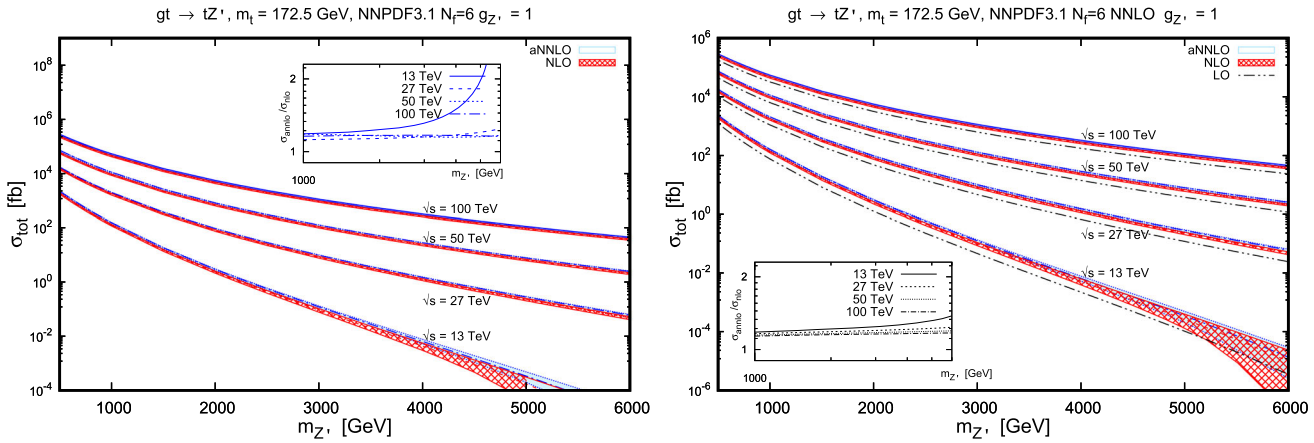

Fig. 18 (Left) Total cross sections for the $gt \to tZ'$ process at NLO and aNNLO as a function of the mass of the Z' for various collider energies. The aNNLO result is obtained using NNPDF3.1 NNLO $n_f = 6$ PDFs, while NLO is obtained using the same PDFs at NLO. (Right) Total cross sections for the $gt \to tZ'$ process at LO, NLO, and aNNLO where all results use NNPDF3.1 NNLO PDFs. In both plots the error bands represent PDF uncertainties at 1-σ C.L., and the inset plots show $\sigma_{aNNLO}/\sigma_{NLO}$ K-factors

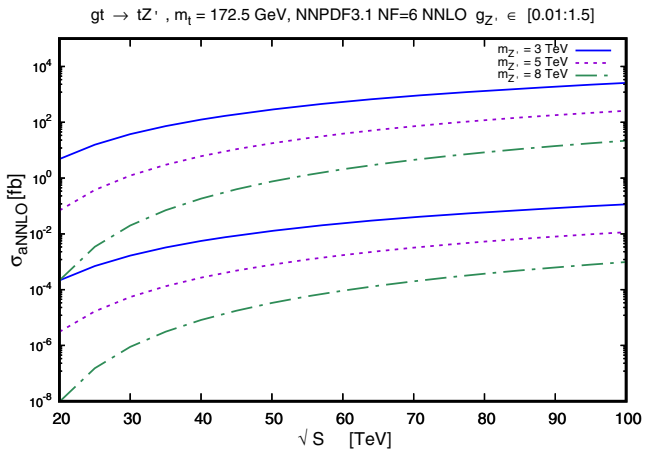

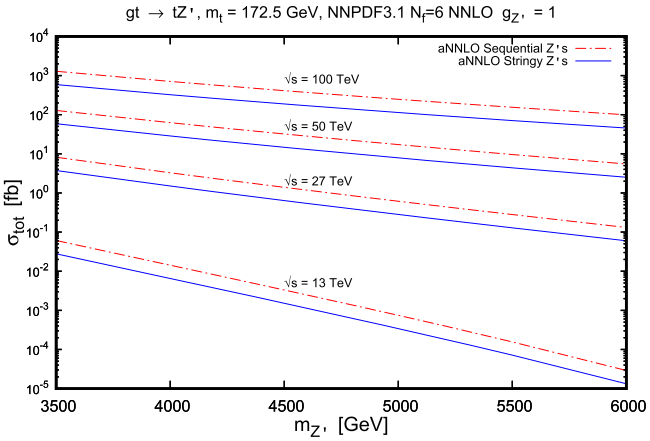

Fig. 19 Left: Scan of the $g_{Z'}$ parameter for the $gt \to tZ'$ process. The plot shows results of the total cross section at aNNLO as a function of collider energy. Bands with different dashing represent Z' mass values of 3, 5, and 8 TeV. Right: Comparison between string-inspired Z's and sequential Z's for different values of the collider energy at aNNLO

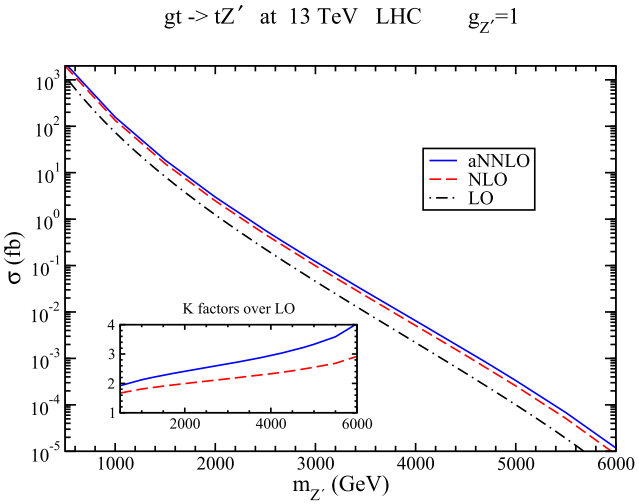

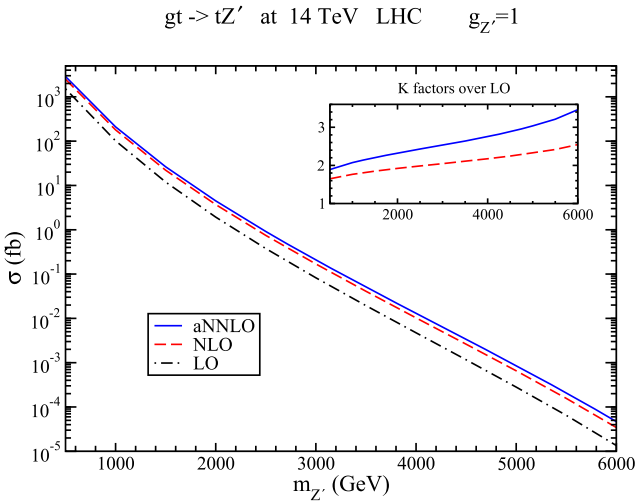

Fig. 20 Total cross section for the $gt \to tZ'$ process at the LHC 13 TeV (left) and 14 TeV (right). LO, NLO and NNLO calculations are obtained using NNPDF3.1 NNLO $n_f = 6$ PDFs

$g_{Z'}$, e.g., $g_{R,L}^{(Z')} = g_{Z'}(g_V \pm g_A)$. In this specific comparison we consider Z' masses larger than 4 TeV because sequential Z's are currently excluded for smaller masses [65,66]. As expected, the shapes in the two models are identical.

Prospects at the LHC at 13 and 14 TeV collision energies are shown in Fig. 20 where the inset plots show the NLO/LO and aNNLO/LO K-factors. Here, LO, NLO, and aNNLO cross sections are all obtained by using NNPDF3.1 NNLO $n_f = 6$ PDFs to show the soft-gluon enhancement in the hard scattering. We note the large effect of the higher-order corrections, which more than triple the LO result for a 6 TeV Z' mass. We also provide numerical values for the $gt \to tZ'$ cross section and K-factors at 13 TeV energy in Table 3 of Appendix C.

Total cross section results as functions of the collider energy up to 100 TeV for different values of $m_{Z'}$ are given in Fig. 21. The inset plot shows the NLO/LO and aNNLO/LO K-factors where NNPDF3.1 NNLO $n_f = 6$ PDFs are used for LO, NLO, and aNNLO calculations. While the cross sections get smaller with increasing Z' mass, the K-factors get larger because this kinematic region is closer to the partonic threshold.

In the left plot of Fig. 22 we illustrate the induced NNPDF3.1 $n_f = 6$ NNLO PDF uncertainty on the σ_{aNNLO} total cross section which we normalize to σ_{LO} to obtain K-factors. Here the LO cross section is also obtained with NNLO PDFs. The large uncertainty of the top-quark NNLO PDF dominates at all collider energies and for every value of $m_{Z'}$. In the plot on the right of Fig. 22 we show the scale

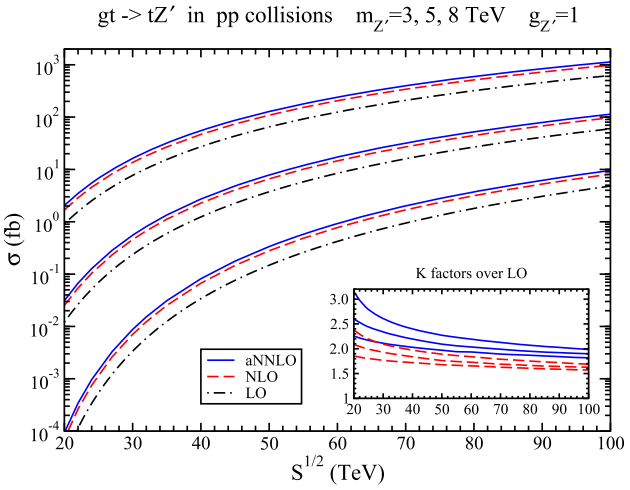

Fig. 21 Total cross sections for the $gt \to tZ'$ process. The plot shows results as a function of collider energy for three choices of Z' mass, 3, 5, and 8 TeV. The inset plot displays K-factors. NNPDF3.1 NNLO $n_f = 6$ PDFs are used for LO, NLO, and aNNLO calculations. Cross sections get smaller with increasing Z' mass while K-factors get larger

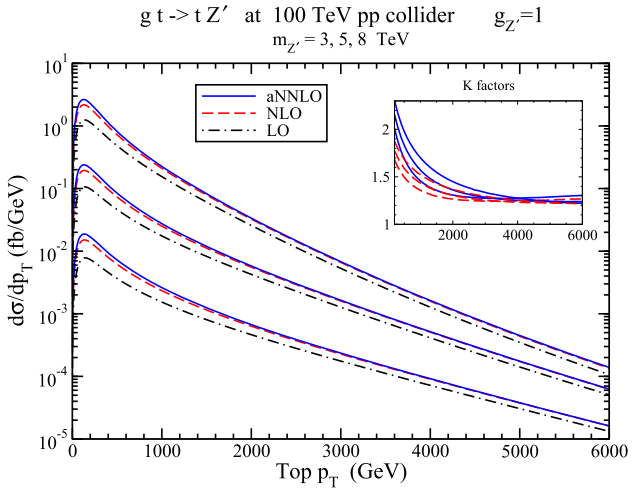

Fig. 23 Top-quark p_T distributions for the $gt \to tZ'$ process at 100 TeV pp collider energy for $m_{Z'} = 3$, 5, and 8 TeV. NNPDF3.1 NNLO $n_f = 6$ PDFs are used for LO, NLO, and aNNLO calculations

uncertainty due to factorization scale variation in $m_{Z'}/2 \leq \mu \leq 2m_{Z'}$. As mentioned in previous sections, the K-factors here are defined as $\sigma_{\text{aNNLO}}(\mu)/\sigma_{\text{LO}}$ where σ_{LO} is obtained using the default central choice $\mu = m_{Z'}$ and NNPDF3.1 $n_f = 6$ NNLO PDFs.

4.4.1 Top-quark p_T distributions for string-inspired Z's

In this section we show the top-quark p_T distributions for this process. Figure 23 shows the top-quark p_T distributions in the $gt \to tZ'$ process at LO, NLO, and aNNLO for different $m_{Z'}$ values at a collider energy of 100 TeV. NNPDF3.1 NNLO $n_f = 6$ PDFs are used for LO, NLO, and aNNLO calculations to emphasize the enhancement in the hard scattering contribution. The K-factors are shown in the inset plot.

5 Conclusions

We have studied tZ' production in various BSM models at hadron colliders. We performed a phenomenological QCD analysis where we scrutinized tZ' production in the presence of FCNC and in the case in which the extra Z' is generated within a low-energy realization of string theory models. We have calculated theoretical predictions for cross sections and top-quark p_T distributions that include higher-order soft-gluon corrections. In particular, theory predictions are obtained at aNNLO in QCD by extending the soft-gluon resummation formalism to the case in which a top quark is

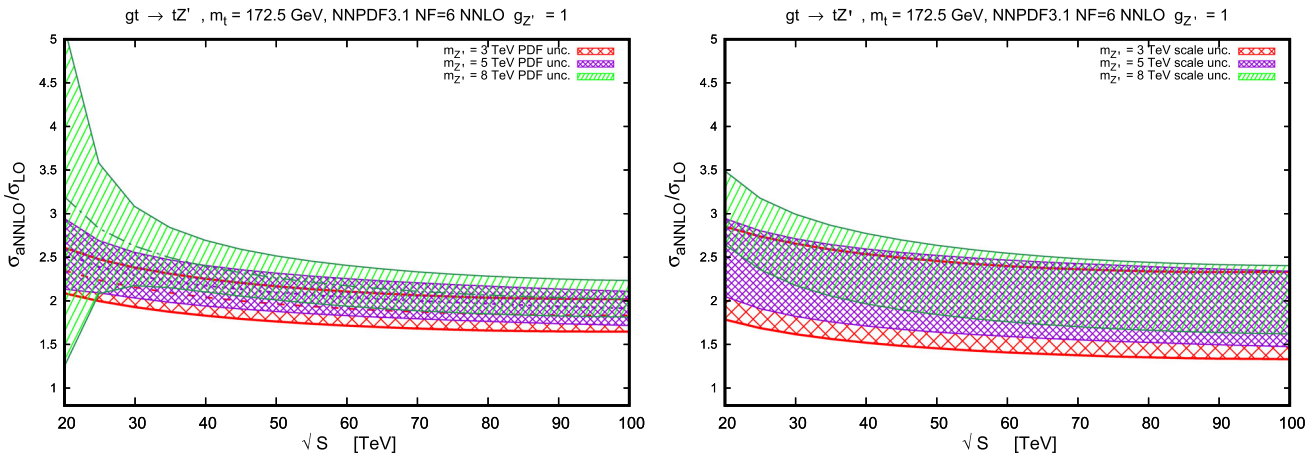

Fig. 22 Left: K-factors for the $gt \to tZ'$ process with NNPDF3.1 $n_f = 6$ PDF uncertainties. The plot shows aNNLO/LO results as a function of $\sqrt{S}$ for three choices of Z' mass, 3, 5, and 8 TeV. Right: K-factors with scale uncertainty bands. Scale variation refers to $m_{Z'}/2 \leq \mu \leq 2m_{Z'}$

produced in association with a heavy neutral vector boson in pp collisions at energies that relevant for the LHC and for future new-generation hadron colliders like FCC-hh and SppC. We have found that QCD corrections due to soft-gluon emissions are considerable and need to be included in precision studies.

We have investigated the impact of uncertainties due to proton PDFs as well as uncertainties due to scale variation. PDFs uncertainties represent the major source of uncertainty in this analysis. Moreover, we explored the parameter space for the BSM models we scrutinized by performing parameter scans and studying the sensitivity of the cross section to parameter changes. We have found that the total tZ' cross section has large sensitivity on the mass of the Z'.

These theoretical results will be useful for tZ' production searches at the LHC and future hadron colliders.

Acknowledgements We thank Gauthier Durieux and Fabio Maltoni for correspondence and suggestions about the use of Madgraph5. The work of M.G. is supported by the National Science Foundation under Grant No. PHY 1820818. The work of N.K. is supported by the National Science Foundation under Grant No. PHY 1820795.

Data Availability Statement This manuscript has no associated data or the data will not be deposited. [Authors' comment: This work is theoretical. We calculated theory predictions for a process involving a particle which has not yet been discovered. Up to now, there is no experimental data for the processes we are considering.]

Funded by SCOAP[3].

A Appendix: PDF uncertainties

The CT14NNLO PDF uncertainties are determined within the Hessian method at 90% C.L., and the CT14NNLO eigenvector sets relative to the positive and negative excursion of the PDF parameters are determined in the QCD global analysis published in Ref. [61]. The induced PDF errors on the cross section are obtained by using the asymmetric formula [67]

$$\delta^+\sigma = \sqrt{\sum_{i=1}^{N_a}\left[\max\left(\sigma_i^{(+)}-\sigma_0,\sigma_i^{(-)}-\sigma_0,0\right)\right]^2},$$

$$\delta^-\sigma = \sqrt{\sum_{i=1}^{N_a}\left[\max\left(\sigma_0-\sigma_i^{(+)},\sigma_0-\sigma_i^{(-)},0\right)\right]^2}, \tag{A.1}$$

in terms of σ_0, the cross section obtained with the best-fit (central) PDF value, and $\sigma_i^{\pm}$, the cross sections for positive and negative variations of the PDF parameters along the i-th eigenvector direction in the N_a-dimensional PDF parameter space. PDF error bands at 68% C.L. are obtained by the rescaling factor 1.645.

For the NNPDF3.1 NNLO PDF uncertainties, the central value F_0 (where F_0 can be a cross section or a PDF) is given by the average and the standard deviation δF is taken over the observable F calculated with each PDF replica set, S_k ($k = 1,\ldots, N_{rep}$) [68–70]

$$F_0 = \langle F\rangle = \frac{1}{N_{rep}}\sum_{k=1}^{N_{rep}} F(S_k)$$

$$\delta F = \sqrt{\frac{1}{N_{rep}-1}\sum_{k=1}^{N_{rep}}(F(S_k)-\langle F\rangle)^2}$$

$$= \sqrt{\frac{N_{rep}}{N_{rep}-1}\left(\langle F^2\rangle-\langle F\rangle^2\right)}. \tag{A.2}$$

The NNPDF3.1 set with $N_f = 6$ and $\alpha_s(m_Z) = 0.118$ which we have used, contains 100 replicas. The 68 % C.L. and 1-σ PDF uncertainties are very similar in absence of non-gaussian behavior of the probability distribution.

B Appendix: Correlations

If $A(f)$ and $B(f)$ are two quantities that depend on a generic PDF f, determined within the Hessian method, the extent of correlation between A and B can be assessed by calculating the correlation cosine

$$\cos\phi_{AB} = \frac{1}{4\Delta A\Delta B}\sum_{k=1}^{n}\hat{A}(f_k)\hat{B}(f_k) \tag{B.1}$$

where

$$\hat{A}(f_k) = \left[A(f_k^+)-A(f_k^-)\right],$$
$$\hat{B}(f_k) = \left[B(f_k^+)-B(f_k^-)\right], \tag{B.2}$$

and the uncertainties on A and B can be obtained by using the symmetric formula

$$\Delta A = \frac{1}{2}\sqrt{\sum_{k=1}^{n}\left[A(f_k^+)-A(f_k^-)\right]^2}. \tag{B.3}$$

The best-fit estimate for A_0 is defined as $A(f_0)$ and $f_k^{\pm}$ represent the n PDF eigenvector sets in the positive and negative direction respectively. When A and B are strongly cor-

related, then $\cos\phi_{AB} \approx 1$. Anticorrelation corresponds to $\cos\phi_{AB} \approx -1$, and uncorrelation to $\cos\phi_{AB} \approx 0$. The simultaneous uncertainty boundaries on A and B, representing the allowed regions, can be obtained with the Lissajous parametric ellipse, defined as

$$A = A_0 + \Delta A \sin(\theta + \phi_{AB})$$
$$B = B_0 + \Delta B \sin\theta \quad \text{(B.4)}$$

where the parameter θ is in the interval $0 < \theta < 2\pi$ (see Ref. [71]).

C Appendix: Additional tables for total cross sections

We provide two tables with aNNLO cross sections with their scale and PDF uncertainties as well as the associated K-factors at 13 TeV LHC energy. Results are given for three choices of Z' mass.

Table 2 shows the aNNLO cross sections for the FCNC process $gu \to tZ'$ with $k_{tuZ'}/\Lambda = 0.01/m_t$. As shown in Sects. 2.4 and 3, the cross sections are proportional to $k^2_{tuZ'}/\Lambda^2$ so it is trivial to recalculate them for any other value of $k_{tuZ'}/\Lambda$.

Table 3 shows the aNNLO cross sections for the process $gt \to tZ'$ with $g_{Z'} = 1$. The dependence of the cross sections on $g_{Z'}$ is given through the formulas in Sects. 2.4 and 3.

Table 2 aNNLO cross sections and aNNLO/LO K-factors for $gu \to tZ'$ with $k_{tuZ'}/\Lambda = 0.01/m_t$ and $m_t = 172.5$ GeV at 13 TeV LHC collider energy. The CT14NNLO PDF uncertainties are calculated at the 68% C.L. The scale uncertainties are obtained by taking up and down variations of the factorization scale μ, $m_{Z'}/2 < \mu < 2m_{Z'}$

$m_{Z'}$ (TeV)	σ_{aNNLO} (fb)	δPDF (CT14NNLO)	δscale	K-factor
1	14.4	± 0.3	$^{+0.3}_{-0.4}$	1.74
3	0.272	$^{+0.025}_{-0.062}$	$^{+0.001}_{-0.006}$	2.24
5	0.00659	$^{+0.00134}_{-0.00086}$	$^{+0.00001}_{-0.00018}$	2.78

Table 3 aNNLO cross sections and aNNLO/LO K-factors for $gt \to tZ'$ with $g_{Z'} = 1$ and $m_t = 172.5$ GeV at 13 TeV LHC collider energy. The NNPDF3.1 $n_f = 6$ PDF uncertainties are determined at the 1-σ C.L. The scale uncertainties are obtained by taking up and down variations of the factorization scale μ, $m_{Z'}/2 < \mu < 2m_{Z'}$

$m_{Z'}$ (TeV)	σ_{aNNLO} (fb)	δPDF(NNPDF3.1)	δscale	K-factor
1	157	± 16	$^{+56}_{-60}$	2.12
3	0.122	± 0.018	$^{+0.021}_{-0.026}$	2.66
5	3.34×10^{-4}	$\pm 1.88 \times 10^{-4}$	$^{+3.7\times10^{-5}}_{-5.3\times10^{-5}}$	3.33

References

1. CMS Collaboration, Measurement of the top quark mass with lepton+jets final states in pp collisions at $\sqrt{s} = 13$ TeV, CMS-PAS-TOP-17-007
2. CMS Collaboration, N. Kovalchuk, Measurement of the top quark mass with lepton+jets final states in pp collisions at $\sqrt{s} = 13$ TeV, in *Proceedings, 10th International Workshop on Top Quark Physics (TOP2017)*, Braga, September 17–22, 2017 (2018). arXiv:1801.05619
3. ATLAS Collaboration, Measurement of the top quark mass in the $t\bar{t} \to$ lepton+jets channel from $\sqrt{s}$=8 TeV ATLAS data, ATLAS-CONF-2017-071
4. HL-LHC, HE-LHC Working Group, P. Azzi et al., Standard Model Physics at the HL-LHC and HE-LHC. arXiv:1902.04070
5. The FCC collaboration, Future Circular Collider, Vol. 1. Physics opportunities, CERN-ACC-2018-0056
6. The FCC Collaboration, Future Circular Collider, Vol. 2. The Lepton Collider (FCC-ee), CERN-ACC-2018-0057
7. The FCC Collaboration, Future Circular Collider, Vol. 3. The Hadron Collider (FCC-hh), CERN-ACC-2018-0058
8. J. Tang et al., Concept for a future super proton–proton collider. arXiv:1507.03224
9. P. Langacker, The physics of heavy Z' gauge bosons. Rev. Mod. Phys. **81**, 1199 (2009). https://doi.org/10.1103/RevModPhys.81.1199, arXiv:0801.1345
10. T.G. Rizzo, Z' phenomenology and the LHC, in *Proceedings of Theoretical Advanced Study Institute in Elementary Particle Physics: Exploring New Frontiers Using Colliders and Neutrinos (TASI 2006)*, Boulder, June 4–30, 2006, pp. 537–575 (2006). arXiv:hep-ph/0610104
11. A. Leike, The phenomenology of extra neutral gauge bosons. Phys. Rep. **317**, 143 (1999). https://doi.org/10.1016/S0370-1573(98)00133-1. arXiv:hep-ph/9805494
12. J.L. Hewett, T.G. Rizzo, Low-energy phenomenology of superstring inspired E(6) models. Phys. Rep. **183**, 193 (1989). https://doi.org/10.1016/0370-1573(89)90071-9
13. Yu. Ya, Komachenko, M.Yu. Khlopov, On manifestation of Z' boson of heterotic string in exclusive neutrino $N \to$ neutrino P0 N processes. Sov. J. Nucl. Phys. **51**, 692 (1990)
14. K.S. Babu, C.F. Kolda, J. March-Russell, Implications of generalized Z-Z-prime mixing. Phys. Rev. D **57**, 6788 (1998). https://doi.org/10.1103/PhysRevD.57.6788. arXiv:hep-ph/9710441
15. J. Adelman, J. Ferrando, C.D. White, NLO QCD corrections to tW' and tZ' production in forward–backward asymmetry models. JHEP **1302**, 091 (2013). https://doi.org/10.1007/JHEP02(2013)091. arXiv:1206.5731
16. B. Fuks, M. Klasen, F. Ledroit, Q. Li, J. Morel, Precision predictions for Z'-production at the CERN LHC: QCD matrix elements, parton showers, and joint resummation. Nucl. B **797**, 322 (2008). https://doi.org/10.1016/j.nuclphysb.2008.01.017. arXiv:0711.0749
17. T. Jezo, M. Klasen, D.R. Lamprea, F. Lyonnet, I. Schienbein, NLO+NLL limits on W' and Z' gauge boson masses in general extensions of the Standard Model. JHEP **1412**, 092 (2014). https://doi.org/10.1007/JHEP12(2014)092. arXiv:1410.4692
18. R. Bonciani, T. Jezo, M. Klasen, F. Lyonnet, I. Schienbein, Electroweak top-quark pair production at the LHC with Z' bosons to NLO QCD in POWHEG. JHEP **1602**, 141 (2016). https://doi.org/10.1007/JHEP02(2016)141. arXiv:1511.08185
19. B. Fuks, R. Ruiz, A comprehensive framework for studying W' and Z' bosons at hadron colliders with automated jet veto resummation. JHEP **1705**, 032 (2017). https://doi.org/10.1007/JHEP05(2017)032. arXiv:1701.05263

20. J.Y. Araz, G. Corcella, M. Frank, B. Fuks, Loopholes in Z searches at the LHC: exploring supersymmetric and leptophobic scenarios. JHEP **1802**, 092 (2018). https://doi.org/10.1007/JHEP02(2018)092. arXiv:1711.06302
21. D. Dicus, T. Stelzer, Z. Sullivan, S. Willenbrock, Higgs boson production in association with bottom quarks at next-to-leading order. Phys. Rev. D **59**, 094016 (1999). https://doi.org/10.1103/PhysRevD.59.094016. arXiv:hep-ph/9811492
22. S. Dawson, A. Ismail, I. Low, Redux on "When is the top quark a parton?". Phys. Rev. D **90**, 014005 (2014). https://doi.org/10.1103/PhysRevD.90.014005. arXiv:1405.6211
23. T. Han, J. Sayre, S. Westhoff, Top-quark initiated processes at high-energy hadron colliders. JHEP **1504**, 145 (2015). https://doi.org/10.1007/JHEP04(2015)145. arXiv:1411.2588
24. M.A.G. Aivazis, J.C. Collins, F.I. Olness, W.-K. Tung, Leptoproduction of heavy quarks. 2. A Unified QCD formulation of charged and neutral current processes from fixed target to collider energies. Phys. Rev. D **50**, 3102 (1994). https://doi.org/10.1103/PhysRevD.50.3102. arXiv:hep-ph/9312319
25. J.C. Collins, Hard scattering factorization with heavy quarks: a general treatment. Phys. Rev. D **58**, 094002 (1998). https://doi.org/10.1103/PhysRevD.58.094002. arXiv:hep-ph/9806259
26. M. Kramer, 1, F.I. Olness, D.E. Soper, Treatment of heavy quarks in deeply inelastic scattering. Phys. Rev. D **62**, 096007 (2000). https://doi.org/10.1103/PhysRevD.62.096007. arXiv:hep-ph/0003035
27. W.-K. Tung, S. Kretzer, C. Schmidt, Open heavy flavor production in QCD: conceptual framework and implementation issues. J. Phys. G **28**, 983 (2002). https://doi.org/10.1088/0954-3899/28/5/321. arXiv:hep-ph/0110247
28. M. Guzzi, P.M. Nadolsky, H.-L. Lai, C.P. Yuan, General-mass treatment for deep inelastic scattering at two-loop accuracy. Phys. Rev. D **86**, 053005 (2012). https://doi.org/10.1103/PhysRevD.86.053005. arXiv:1108.5112
29. N. Kidonakis, A. Belyaev, FCNC top quark production via anomalous tqV couplings beyond leading order. JHEP **0312**, 004 (2003). https://doi.org/10.1088/1126-6708/2003/12/004. arXiv:hep-ph/0310299
30. N. Kidonakis, Higher-order corrections for tZ production via anomalous couplings. Phys. Rev. D **97**, 034028 (2018). https://doi.org/10.1103/PhysRevD.97.034028. arXiv:1712.01144
31. M. Forslund, N. Kidonakis, Associated production of a top quark with a photon via anomalous couplings. Phys. Rev. D **98**, 074017 (2018). https://doi.org/10.1103/PhysRevD.98.074017. arXiv:1808.09014
32. N. Kidonakis, NNNLO soft-gluon corrections for the top-antitop pair production cross section. Phys. Rev. D **90**, 014006 (2014). https://doi.org/10.1103/PhysRevD.90.014006. arXiv:1405.7046
33. N. Kidonakis, NNNLO soft-gluon corrections for the top-quark p_T and rapidity distributions. Phys. Rev. D **91**, 031501 (2015). arXiv:1411.2633. https://doi.org/10.1103/PhysRevD.91.031501
34. N. Kidonakis, The top quark forward-backward asymmetry at approximate N^{3}LO. Phys. Rev. D **91**, 071502 (2015). https://doi.org/10.1103/PhysRevD.91.071502. arXiv:1501.01581
35. N. Kidonakis, NNLL resummation for s-channel single top quark production. Phys. Rev. D **81**, 054028 (2010). https://doi.org/10.1103/PhysRevD.81.054028. arXiv:1001.5034
36. N. Kidonakis, Two-loop soft anomalous dimensions for single top quark associated production with a W^- or H^-. Phys. Rev. D **82**, 054018 (2010). https://doi.org/10.1103/PhysRevD.82.054018. arXiv:1005.4451
37. N. Kidonakis, Next-to-next-to-leading-order collinear and soft gluon corrections for t-channel single top quark production. Phys. Rev. D **83**, 091503 (2011). https://doi.org/10.1103/PhysRevD.83.091503. arXiv:1103.2792
38. N. Kidonakis, Single-top transverse-momentum distributions at approximate NNLO. Phys. Rev. D **93**, 054022 (2016). https://doi.org/10.1103/PhysRevD.93.054022. arXiv:1510.06361
39. N. Kidonakis, Soft-gluon corrections for tW production at N^{3}LO. Phys. Rev. D **96**, 034014 (2017). https://doi.org/10.1103/PhysRevD.96.034014. arXiv:1612.06426
40. N. Kidonakis, Soft-gluon corrections in top-quark production. Int. J. Mod. Phys. A **33**, 1830021 (2018). https://doi.org/10.1142/S0217751X18300211. arXiv:1806.03336
41. C. Corianò, A.E. Faraggi, M. Guzzi, Searching for extra Z-prime from strings and other models at the LHC with leptoproduction. Phys. Rev. D **78**, 015012 (2008). https://doi.org/10.1103/PhysRevD.78.015012. arXiv:0802.1792
42. A.E. Faraggi, M. Guzzi, Extra Z' s and W' s in heterotic-string derived models. Eur. Phys. J. C **75**, 537 (2015). https://doi.org/10.1140/epjc/s10052-015-3763-4. arXiv:1507.07406
43. N. Kidonakis, G.F. Sterman, Resummation for QCD hard scattering. Nucl. Phys. B **505**, 321 (1997). https://doi.org/10.1016/S0550-3213(97)00506-3. arXiv:hep-ph/9705234
44. N. Kidonakis, Two-loop soft anomalous dimensions and NNLL resummation for heavy quark production. Phys. Rev. Lett. **102**, 232003 (2009). https://doi.org/10.1103/PhysRevLett.102.232003. arXiv:0903.2561
45. N. Kidonakis, Soft anomalous dimensions for single-top production at three loops. Phys. Rev. D **99**, 074024 (2019). https://doi.org/10.1103/PhysRevD.99.074024. arXiv:1901.09928
46. G.F. Sterman, Summation of large corrections to short distance hadronic cross-sections. Nucl. Phys. B **281**, 310 (1987). https://doi.org/10.1016/0550-3213(87)90258-6
47. S. Catani, L. Trentadue, Resummation of the QCD perturbative series for hard processes. Nucl. Phys. B **327**, 323 (1989). https://doi.org/10.1016/0550-3213(89)90273-3
48. CMS Collaboration, Search for high-mass resonances in dilepton final states in proton-proton collisions at $\sqrt{s} = 13$ TeV. JHEP **1806**, 120 (2018). https://doi.org/10.1007/JHEP06(2018)120. arXiv:1803.06292
49. ATLAS Collaboration, Search for high-mass dilepton resonances using 139 fb^{-1} of pp collision data collected at $\sqrt{s}$ =13 TeV with the ATLAS detector. Phys. Lett. B **796**, 68 (2019). https://doi.org/10.1016/j.physletb.2019.07.016. arXiv:1903.06248
50. B.H. Li, Y. Zhang, C.S. Li, J. Gao, H.X. Zhu, Next-to-leading order QCD corrections to tZ associated production via the flavor-changing neutral-current couplings at hadron colliders. Phys. Rev. D **83**, 114049 (2011). https://doi.org/10.1103/PhysRevD.83.114049. arXiv:1103.5122
51. J. Pumplin, D.R. Stump, J. Huston, H.-L. Lai, P.M. Nadolsky, W.K. Tung, New generation of parton distributions with uncertainties from global QCD analysis. JHEP **0207**, 012 (2002). https://doi.org/10.1088/1126-6708/2002/07/012. arXiv:hep-ph/0201195
52. J. Alwall, R. Frederix, S. Frixione, V. Hirschi, F. Maltoni, et al., The automated computation of tree-level and next-to-leading order differential cross sections, and their matching to parton shower simulations. JHEP **1407**, 079 (2014). https://doi.org/10.1007/JHEP07(2014)079. arXiv:1405.0301
53. C. Degrande, F. Maltoni, J. Wang, C. Zhang, Automatic computations at next-to-leading order in QCD for top-quark flavor-changing neutral processes. Phys. Rev. D **91**, 034024 (2015). https://doi.org/10.1103/PhysRevD.91.034024. arXiv:1412.5594
54. G. Durieux, F. Maltoni, C. Zhang, Global approach to top-quark flavor-changing interactions. Phys. Rev. D **91**, 074017 (2015). https://doi.org/10.1103/PhysRevD.91.074017. arXiv:1412.7166
55. A.D. Martin, W.J. Stirling, R.S. Thorne, G. Watt, Parton distributions for the LHC. Eur. Phys. J. C **63**, 189 (2009). https://doi.org/10.1140/epjc/s10052-009-1072-5. arXiv:0901.0002

56. CMS Collaboration, Search for associated production of a Z boson with a single top quark and for tZ flavour-changing interactions in pp collisions at sqrt(s) = 8 TeV, CMS-PAS-TOP-12-039
57. ATLAS Collaboration, G. Aad et al., Search for flavour-changing neutral current top-quark decays to qZ in pp collision data collected with the ATLAS detector at $\sqrt{s} = 8$ TeV. Eur. Phys. J. C **76**, 12 (2016). https://doi.org/10.1140/epjc/s10052-015-3851-5. arXiv:1508.05796
58. CMS Collaboration, V. Khachatryan et al., Search for anomalous single top quark production in association with a photon in pp collisions at $\sqrt{s} = 8$ TeV. JHEP **1604**, 035 (2016). https://doi.org/10.1007/JHEP04(2016)035. arXiv:1511.03951
59. H. Khanpour, S. Khatibi, M. Khatiri Yanehsari, M. Mohammadi Najafabadi, Single top quark production as a probe of anomalous $tq\gamma$ and tqZ couplings at the FCC-ee. Phys. Lett. B **775**, 25 (2017). https://doi.org/10.1016/j.physletb.2017.10.047. arXiv:1408.2090
60. W.S. Hou, M. Kohda, T. Modak, Search for tZ' associated production induced by tcZ' couplings at the LHC. Phys. Rev. D **96**, 015037 (2017). https://doi.org/10.1103/PhysRevD.96.015037 arXiv:1702.07275
61. S. Dulat, T.-J. Hou, J. Gao, M. Guzzi, J. Huston, P. Nadolsky et al., New parton distribution functions from a global analysis of quantum chromodynamics. Phys. Rev. D **93**, 033006 (2016). https://doi.org/10.1103/PhysRevD.93.033006. arXiv:1506.07443
62. F. Petriello, S. Quackenbush, Measuring Z' couplings at the CERN LHC. Phys. Rev. D **77**, 115004 (2008). https://doi.org/10.1103/PhysRevD.77.115004. arXiv:0801.4389
63. F. Petriello, S. Quackenbush, K.M. Zurek, The invisible Z' at the CERN LHC. Phys. Rev. D **77**, 115020 (2008). https://doi.org/10.1103/PhysRevD.77.115020. arXiv:0803.4005
64. NNPDF Collaboration, R.D. Ball et al., Parton distributions from high-precision collider data. Eur. Phys. J. C **77**, 663 (2017). https://doi.org/10.1140/epjc/s10052-017-5199-5. arXiv:1706.00428
65. M. Aaboud et al. [ATLAS Collaboration], Search for new high-mass phenomena in the dilepton final state using 36 fb^{-1} of proton-proton collision data at $\sqrt{s} = 13$ TeV with the ATLAS detector. JHEP **1710**, 182 (2017). https://doi.org/10.1007/JHEP10(2017)182. arXiv:1707.02424
66. CMS Collaboration [CMS Collaboration], Search for a high-mass resonance decaying into a dilepton final state in 13 fb^{-1} of pp collisions at $\sqrt{s} = 13$ TeV CMS-PAS-EXO-16-031
67. P.M. Nadolsky, Z. Sullivan, PDF uncertainties in WH production at Tevatron. eConf **C010630**, P510 (2001). arXiv:hep-ph/0110378
68. S. Alekhin et al., The PDF4LHC Working Group Interim Report. arXiv:1101.0536
69. A. Buckley, J. Ferrando, S. Lloyd, K. Nordström, B. Page, M. Rüfenacht, M. Schönherr, G. Watt, LHAPDF6: parton density access in the LHC precision era. Eur. Phys. J. C **75**, 132 (2015). https://doi.org/10.1140/epjc/s10052-015-3318-8. arXiv:1412.7420
70. G. Watt, Parton distribution function dependence of benchmark Standard Model total cross sections at the 7 TeV LHC. JHEP **1109**, 069 (2011). https://doi.org/10.1007/JHEP09(2011)069. arXiv:1106.5788
71. J. Pumplin, D. Stump, R. Brock, D. Casey, J. Huston, J. Kalk et al., Uncertainties of predictions from parton distribution functions. 2. The Hessian method. Phys. Rev. D **65**, 014013 (2001). https://doi.org/10.1103/PhysRevD.65.014013. arXiv:hep-ph/0101032